European Journal of Pharmaceutics and Biopharmaceutics 144 (2019) 252–265

Contents lists available at ScienceDirect

European Journal of Pharmaceutics and Biopharmaceutics

journal homepage: www.elsevier.com/locate/ejpb

Simulated biological fluid exposure changes nanoceria's surface properties but not its biological response

Robert A. Yokel[a,*], Matthew L. Hancock[b,2], Benjamin Cherian[b,1], Alexandra J. Brooks[b,3], Marsha L. Ensor[a,4], Hemendra J. Vekaria[c,d,5], Patrick G. Sullivan[c,d,6], Eric A. Grulke[b,7]

[a] Pharmaceutical Sciences, University of Kentucky, Lexington, KY 40536-0596, United States
[b] Chemical and Materials Engineering, University of Kentucky, Lexington, KY 40506-0046, United States
[c] Spinal Cord & Brain Injury Research Center, University of Kentucky, Lexington, KY 40536-0509, United States
[d] Department of Neuroscience, University of Kentucky, Lexington, KY 40536-0509, United States

ARTICLE INFO

Keywords:
A549 cells
Body fluids
Caco-2 cells
Cellular respiration
Cerium
Engineered nanoparticles
Hydrodynamic diameter
Microscopy, electron, transmission
Nanoceria
Nanoparticle corona
Spectroscopy, Fourier transform infrared
Thermogravimetric analysis
X-ray diffraction

ABSTRACT

Nanoscale cerium dioxide (nanoceria) has industrial applications, capitalizing on its catalytic, abrasive, and energy storage properties. It auto-catalytically cycles between Ce^{3+} and Ce^{4+}, giving it pro-and anti-oxidative properties. The latter mediates beneficial effects in models of diseases that have oxidative stress/inflammation components. Engineered nanoparticles become coated after body fluid exposure, creating a corona, which can greatly influence their fate and effects. Very little has been reported about nanoceria surface changes and biological effects after pulmonary or gastrointestinal fluid exposure. The study objective was to address the hypothesis that simulated biological fluid (SBF) exposure changes nanoceria's surface properties and biological activity. This was investigated by measuring the physicochemical properties of nanoceria with a citric acid coating (size; morphology; crystal structure; surface elemental composition, charge, and functional groups; and weight) before and after exposure to simulated lung, gastric, and intestinal fluids. SBF-exposed nanoceria biological effect was assessed as A549 or Caco-2 cell resazurin metabolism and mitochondrial oxygen consumption rate. SBF exposure resulted in loss or overcoating of nanoceria's surface citrate, greater nanoceria agglomeration, deposition of some SBF components on nanoceria's surface, and small changes in its zeta potential. The engineered nanoceria and SBF-exposed nanoceria produced no statistically significant changes in cell viability or cellular oxygen consumption rates.

Abbreviations: DLS, Dynamic light scattering; EDS, Energy-dispersive X-ray spectroscopy; ENP, Engineered nanoparticle; FaSSGF, Fasted-state simulated gastric fluid; FeSSGF, Fed-state simulated gastric fluid; FaSSIF, Fasted-state simulated intestinal fluid; FeSSIF, Fed-state simulated intestinal fluid; FTIR, Fourier-transform infrared spectroscopy; GIF, Gastrointestinal fluid; OCR, Oxygen consumption rate; SBF, Simulated body fluid (an inclusive term for FaSSGF, FeSSGF, FaSSIF, FeSSIF, and SLF); SLF, Simulated lung fluid; TEM, Transmission electron microscopy; TGA, Thermogravimetric analysis; XRD, Powder X-ray diffraction

* Corresponding author at: Department of Pharmaceutical Sciences, University of Kentucky Academic Medical Center, 335 Todd (College of Pharmacy) Building, 789 S. Limestone, Lexington, KY 40536-0596, United States.
E-mail addresses: ryokel@uky.edu (R.A. Yokel), matthew.hancock@uky.edu (M.L. Hancock), cherianb@vcu.edu (B. Cherian), alexandra.brooks@uky.edu (A.J. Brooks), ml.ensor@uky.edu (M.L. Ensor), hemendravekaria@uky.edu (H.J. Vekaria), patsullivan@uky.edu (P.G. Sullivan), eric.grulke@uky.edu (E.A. Grulke).
[1] Virginia Commonwealth University, Richmond, VA 23284-2006, United States.
[2] Chemical and Materials Engineering Department, A215 ASTeCC, University of Kentucky, Lexington, KY 40506-0046, United States.
[3] Chemical and Materials Engineering Department, University of Kentucky, Lexington, KY 40506-0046, United States.
[4] Department of Pharmaceutical Sciences, University of Kentucky Academic Medical Center, 364 Todd (College of Pharmacy) Building, Lexington, KY 40536-0596, United States.
[5] Spinal Cord & Brain Injury Research Center, B436 BBSRB, University of Kentucky, Lexington, KY 40536-0509, United States.
[6] Spinal Cord & Brain Injury Research Center, 475 BBSRB, University of Kentucky, Lexington, KY 40536-0509, United States.
[7] Chemical and Materials Engineering Department, 763H FPAT, University of Kentucky, Lexington, KY 40506-0046, United States.

https://doi.org/10.1016/j.ejpb.2019.09.023
Received 5 April 2019; Received in revised form 26 August 2019; Accepted 26 September 2019
Available online 26 September 2019
0939-6411/

1. Introduction

Engineered nanoparticles (ENPs) are typically coated to enhance their stability (deter agglomeration) and/or target their distribution. Once they enter the biological milieu, the coating may be removed, altered by body fluids, or overcoated by body fluid components, creating a corona. The chemistry and morphology of the nanoparticle surface, what cells "see", can greatly influence its fate and effects [1,2]. For many nanoparticles the influence of biological fluids to remove, alter, or overcoat the applied coatings has not been well characterized.

Studies of Ag nanoparticles exposed to oral and gastrointestinal fluids (GIFs) have been reported [3–6]. Reports have described the effect of GIFs on SiO_2 and ZnO nanoparticles and resultant particle effects on Caco-2 cells [7–9] and the effect of GIFs on CuO nanoparticles and small intestine cell response [10]. GIF exposure caused agglomeration/deagglomeration of Ag, SiO_2, Al^0, and γ-Al_2O_3 nanoparticles [3–5,8,11]. With the exception of changes in the zeta potential [10] or surface elemental analysis [11] that were not assessed for biological effect, nanoparticle surface properties were not reported in these studies.

Exposure of ENPs to GIFs or their components can change their surface properties. The surface charge of nanotitania and nanosilica became more electronegative after pancreatin and bile extract exposure [12]. Fourier-transform infrared spectroscopy (FTIR) revealed protein and bile salt adsorption on nanotitania and nanosilica surfaces. Nanotitania cell toxicity was attributed to the bile salt adsorption. Incubation of Fe_3O_4 nanoparticles with bread in simulated salivary and GIFs resulted in size, surface charge, and protein corona changes, resulting in morphological changes (an increase in the number of apical membrane vesicles) and greater Caco-2 uptake of exposed NPs [13]. Exposure of $CdSe_{core}/ZnS_{shell}$ quantum dots to GIFs altered the polyethylene glycol coating, revealed by FTIR. The effect on biological response was not reported [14]. Silicon carbide and TiC nanoparticle exposure to human reconstituted gastric fluid resulted in surface carbon and nitrogen adsorption [15]. The surface and pore structure of mesoporous SiO_2 particles was altered by exposure to salivary and GIF. The effect on biological response was not reported [16].

Much less work has been reported with simulated lung fluids (SLFs). Nanoscale ZnO, CuO, Fe_3O_4, TiO_2, and CeO_2 aggregated in SLFs, including pulmonary artificial lysosomal fluid and Gamble solution. Nanoscale CeO_2 dissolution was 5.5% after two h in a gastric fluid, < 0.2% after two h in an *in vitro* gastric and four h in an *in vitro* intestinal fluid, and none after 24 h in artificial lysosomal fluid or Gamble's solution [17]. Exposure of nanoscale CeO_2, silica-coated CeO_2, $BaSO_4$, and ZnO to rat concentrated bronchoalveolar lavage fluid resulted in agglomerated particles with increased conductance, a negative surface charge (−19 to −15 mV in water), and a corona containing nine identified proteins [18]. The effect on biological response of body-fluid exposed NPs in these two studies was not reported.

Nanoceria (nanoscale cerium dioxide, ceria, CeO_2) is auto-catalytically redox active, cycling between Ce^{3+} and Ce^{4+}. It has a high oxygen storage capacity. Oxygen vacancies in its cubic fluorite structure allow it to easily accept and donate oxygen without significantly altering its geometry. These properties are described in detail in [19]. It displays superoxide dismutase and catalase mimetic activity. It has commercial applications and therapeutic potential for conditions with an oxidative stress/inflammation component [20]. Nanoceria has been shown to have beneficial effects in animal models of cardiomyopathy [21], ventricular hypertrophy [22], cardiac toxicity [23], ovarian cancer [24], pancreatic cancer [25], ischemic stroke [26], retinal degeneration [27], sepsis [28], and hypobaric hypoxia [29]. It has been shown to promote wound healing [30] and improve microvascular function in a model of hypertension [31]. Studies have shown that it can improve the reproductive system of aged and diabetic male rats [32,33] and provide protection against radiation-induced gastric, lung, salivary, dermatologic, and bone marrow toxicity [34–37], and endometriosis [38]. It has been shown beneficial in rodent models of multiple sclerosis, amyotrophic lateral sclerosis, Alzheimer's disease, Parkinson's disease, diabetic neuropathy, traumatic brain injury, and intracerebral hemorrhage [39–46]. It has been shown to reduce adverse brain effects of diesel exhaust exposure [47], ethanol- and stress-induced gastric lesions [48,49], chemical-induced hepatic and pancreatic toxicity [50,51], and ischemia-induced hepatic reperfusion injury [52]. It reduced weight gain [53] and obesity-related inflammatory effects [54]. However, there is concern about potential adverse effects from nanoceria environmental exposure (e.g., from its use as a diesel fuel additive [55]) and occupational exposure [56]. Adverse effects from *in vivo* pulmonary exposure have been demonstrated [57–61].

Cell response to ENPs is dependent on particle physicochemical properties such as size, surface charge, and morphology. Consequently, alterations in these characteristics can lead to favorable or adverse outcomes. For example, application of a surface coating, such as citrate, is routinely conducted to provide biocompatibility and deter agglomeration by providing a charged surface [62,63]. Proteins can coat ENPs to form a corona [1] and be subsequently displaced by other proteins or removed. For example, nanoceria reversibly adsorbs albumin. Albumin interacts with nanoceria in blood due to its prevalence but would be replaced over time by fibrinogen that has a higher affinity [64,65]. These alterations can change the particle surface charge [66]. Aside from two studies ([17;18]) we are not aware of reports of the effect of lung or GIFs on nanoceria. As noted, *in vivo* interactions and resulting protein corona formation are not well understood and will be a focus in advancing our knowledge of nanoceria's potential biomedical applications [20].

This study investigated the effects of human SLF and GIFs on nanoceria surface properties and the effect of the simulated body fluid (SBF)-exposed nanoceria on cell viability and oxygen consumption, to test the hypothesis that exposure to SBFs results in surface changes that affect cell response. It was anticipated that exposure to these SBFs would change the surface charge and coating of citrate-coated nanoceria, which might change cell response to the altered nanoceria. Nanoceria was synthesized by a hydrothermal method, citrate coated, purified by centrifugation and dialysis against water, and extensively characterized to determine its physicochemical identity. It was exposed to simulated lung, gastric, and intestinal fluids, and then again extensively characterized. The SBF-exposed nanoceria was isolated and its effect on the viability and oxygen consumption rate of relevant cells assessed (A549 for SLF-exposed nanoceria and Caco-2 for simulated gastric- and intestinal fluid-exposed nanoceria) to determine its biological identity.

2. Materials and methods

2.1. Materials

The chemicals, their sources, and purity were: acetic acid (glacial), Fisher Scientific, 100%; calcium chloride dihydrate, Fisher Scientific, USP/FCC; cerium nitrate hexahydrate, Fluka Analytical, ≥ 99%; citric acid monohydrate, Fisher Chemical, 100%; citric acid trisodium salt dihydrate, VWR, ≥ 99%; disodium hydrogen phosphate, Fisher Scientific, ACS grade; lecithin from egg, MP Biomedicals, ≥ 96%; hydrochloric acid, Fisher Reagent, 37% ACS grade; lipopolysaccharide E. Coli 0127:B8 (LPS), Sigma, ≥ 500,000 EU/mg; magnesium chloride, Strem Chemicals, 97.5%; maleic acid, TCI, 99%; pepsin, MP Biomedicals; potassium chloride, Sigma, ~ 99%; resazurin, sodium salt, Sigma, ~ 80% dye content; sodium acetate, Sigma Aldrich, ≥ 99%; sodium chloride, Sigma, ≥ 99%; sodium hydrogen carbonate, EM, 98.8%; sodium hydroxide, Fisher Chemical, 98.8%; sodium oleate, TCI, > 97%; sodium sulfate, Sigma Aldrich, ≥ 99%; sodium taurocholate hydrate, Alfa Aesar, 96%; and Triton-X 100 (Biorad). Oligomycin, (4 (trifluoromethoxy) phenyl) carbonohydrazonoyl dicyanide (FCCP) and rotenone were obtained from Biomol. Antimycin A was

obtained from Sigma. Regenerated cellulose dialysis tubing that allows up to 12,000 to 14,000 MW passage was from Ward's Science, West Henrietta, NY. Two % cow milk was used. A549 cells were obtained from Dr. Jill Kolesar, College of Pharmacy, University of Kentucky. Caco-2 cells were obtained from Dr. Kyungbo Kim, College of Pharmacy, University of Kentucky. The identity of both cell lines was verified by the University of Arizona Genetics Core. MEM and DMEM (Gibco), phosphate-free DMEM (Gibco), and low endotoxin FBS (Gibco) were used.

2.2. Methods

2.2.1. Nanoceria synthesis

Nanoceria was synthesized following a hydrothermal method [67]. The goal was to synthesize particles that were large enough to isolate and purify by centrifugation and washing. An aqueous solution containing 35 mL of 6 M sodium hydroxide and 5 mL of 0.05 M cerium nitrate hexahydrate was combined and stirred for 30 min at 350 rpm. The contents were then transferred to an autoclave and heated for 24 h at 180 °C, followed by cooling at room temperature for 24 h. The resulting suspension containing cerium oxide and sodium nitrate was centrifuged at 4200 rpm for 15 min, then washed and repeated three times. The cerium oxide pellet was dispersed and dialyzed against 10 volumes (relative to the nanoceria dispersion) of deionized water for 72 h at 350 rpm (changed every 24 h) to remove excess salt and cerium ions. The nanoceria suspension was centrifuged at 4200 rpm for 15 min, washed and repeated three times, and then dried overnight at 80 °C.

2.2.2. Citrate layer application

Approximately 0.3 g of nanoceria was added to a beaker containing 200 mL of 0.05 M citric acid adjusted to pH 4.5, stirred for 24 h, then centrifuged at 4200 rpm for 15 min. The supernatant was decanted, the citrate-coated particles washed with deionized water three times, then dried at 80 °C overnight. The citrate-coated nanoceria was characterized as described below.

2.2.3. Characterization of non-coated, citrate-coated, and SBF-exposed nanoceria

Powder X-ray diffraction (XRD; Bruker D8 Advance A25 with Cu source) was performed on a 10 mg sample to determine its crystal structure. The crystal planes of the peaks were assigned as described [68]. Selected area electron diffraction was also conducted. Nanoceria was coated on copper grids (300 mesh, lacey carbon #01895, from Ted Pella, Redding, CA) by brief immersion in the nanoceria dispersion to determine primary particle morphology, size, and surface elemental composition. This was conducted by transmission electron microscopy (TEM) and scanning transmission electron microscopy (STEM) using a Thermo Scientific Talos F200X operated at 200 keV and equipped with a 4 silicon drift detector (SDD)-based energy dispersive x-ray spectroscopy (EDS) system for chemical composition analysis and surface elemental distribution mapping. The TEM images are recorded on a Ceta CCD camera. The polygon tool of ImageJ was used to outline 231 particles from five TEM images of citrate-coated nanoceria. Geometric comparison of the square root of area vs. Feret diameter demonstrated that the particles were near cubic. To determine hydrodynamic diameter by dynamic light scattering (DLS) and surface charge as zeta potential, one mg of the dried solid was dispersed in 2 mL of deionized water, facilitated by bath sonication for five min, in a cuvette. A 90Plus Nanoparticle Size Distribution Analyzer (Brookhaven Instruments Corporation, Holtsville, NY) and Litesizer™ 500 Particle Analyzer (Anton Paar, Ashland, VA), respectively, were used. Hydrodynamic diameter was determined from five consecutive five-minute determinations. The zeta potential was determined multiple times from pH 1 to 12. Fourier transform infrared spectroscopy (FTIR) was conducted on the dried nanoceria (Nicolet 6700) to identify surface functional groups by their vibration-induced peaks in the infrared spectrum. Three scans were obtained for each material. FTIR peak assignments were: −C−H, $-CH_2$, and $-CH_3$ 1000 to 1500; C−O− ~ 1100; −C−H 1350 to 1480; −COOH ~ 1380 and 1540; −N−O ~ 1650; C═O 1670 to 1820; and −OH between 3000 and 3600 cm^{-1}. Thermogravimetric analysis (TGA; Perkin Elmer TGA7) was performed on 10 to 15 mg samples to determine the extent of citrate and SBF-deposited surface coatings. Nitrogen was used as an inert gas purge. The temperature was held at 125 °C for 30 min to release adsorbed water, then raised 10 °C/min above 125 °C. Increasing the temperature causes neighboring surface hydroxyls to lose water and pyrolyzes organic compounds from the nanoceria surfaces.

2.2.4. SBF preparation

Five SBFs; lung fluid (Gamble's solution, which represents the interstitial fluid deep within the lung, as the SLF), fasted-state simulated gastric fluid (FaSSGF), fed-state simulated middle gastric fluid (FeSSGF), fasted-state simulated intestinal fluid (FaSSIF), and fed-state simulated middle intestinal fluid (FeSSIF) were prepared as described, with modifications [69–71]. Preparation of the FeSSIF deviated from the [69] formula by exclusion of glyceryl monocholate and from the [71] formula by exclusion of glyceryl monooleate because they prevented isolation of washed, dried nanoceria amenable to the characterization described above. The glyceryl salt and sodium oleate were excluded from the Caco-2 cell FeSSIF medium because their inclusion killed the cells. The SBFs were sterilized by 0.2 μm filtration.

2.2.5. SBF nanoceria exposure

Nanoceria (70 mg) and SBF (15 mL) in a 25 mL centrifuge tube were agitated on an orbital shaker (INNOVA 4000, New Brunswick Scientific, Edison, NJ) at 250 rpm and 37 °C. Exposure to SLF was three h, gastric fluids two h, and intestinal fluids six h, each conducted in three independent replications. After exposure, the dispersions were centrifuged at 3500 rpm for 10 min, washed with deionized water three times, dried overnight at 80 °C, and characterized as described above.

2.2.6. Assessment of nanoceria effect on cell metabolism before and after SBF exposure

To quantify cell metabolism, A549 cells were grown in 24 well plates in DMEM with 10% FBS. Caco-2 cells were grown in 24 well plates in Eagle's MEM with 20% FBS. The resazurin (AKA alamarBlue®) assay was used to assess viability of A549 cells to citrate-coated nanoceria that had not been SLF exposed as well as SLF-exposed nanoceria, and Caco-2 cells to nanoceria before and after simulated gastric and intestinal fluid exposure. The cells were grown to near confluence then washed three times (with phosphate-free DMEM) to remove cell culture growth medium. They were then exposed to nanoceria (0, 1, 5, 20, and 100 μg/cm^2 cell culture dish area, equivalent to 0, 3.8, 19, 76, and 380 μg/ml), that had been SBF-exposed, dispersed by sonication in the same SBF to maintain the nanoceria surface coating (corona) acquired during SBF exposure. Exposure duration was three, two, or six h for lung-, gastric fluid-, and intestinal fluid-exposed nanoceria, respectively. They were also exposed to citrate-coated nanoceria that had not been SBF exposed, introduced as an *iso*-osmotic dispersion in citric acid at pH 7.4, dispersed in phosphate-free DMEM. The cells were then washed three times (with PBS), exposed to 18.75 (for A549 cells) or 25 μg/ml (for Caco-2 cells) resazurin in MEM containing 10% FBS. Absorbance readings were obtained after one and two h. Addition of 100 μg/ml citrate-coated nanoceria to resorufin (the resazurin reduction product) did not alter resorufin fluorescence, compared to citric acid addition, suggesting nanoceria does not interfere with the resazurin assay. A549 cells tolerated SLF exposure. Caco-2 cells did not tolerate exposure to 100% of the simulated gastric or intestinal fluids. It was necessary to include some cell culture medium with these four SBFs to avoid very low viability. Gastric and intestinal SBFs were mixed with DMEM that was phosphate free (to avoid nanoceria phosphate complexation) and in the absence of FBS (to avoid nanoceria protein adherence [72]). Due to the low pH (1.6) of FaSSGF we were unable to

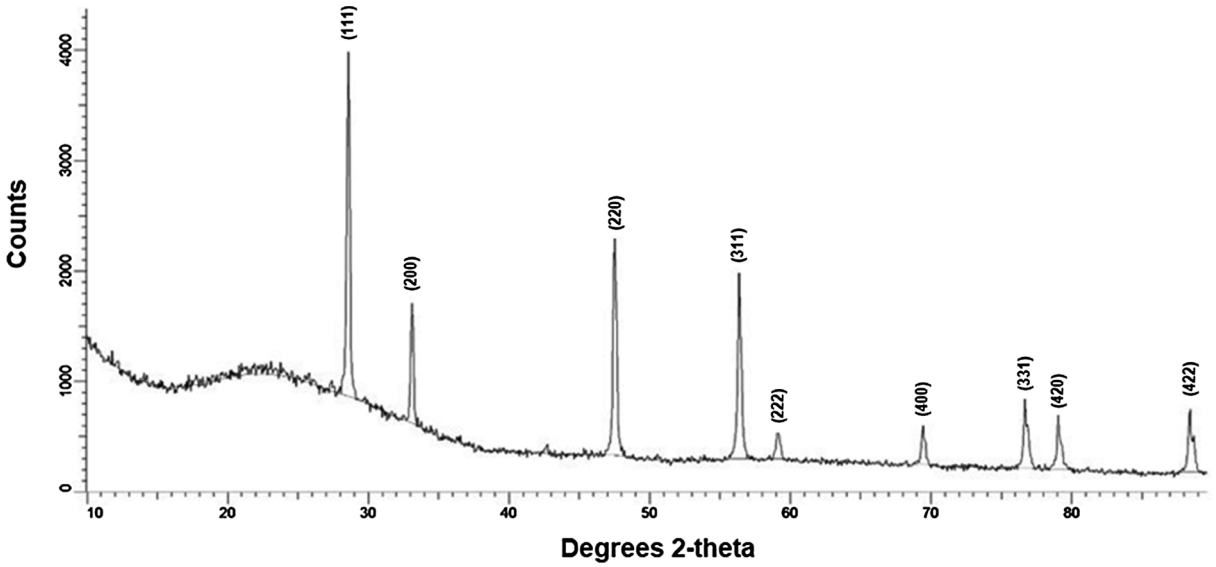

Fig. 1. X-ray powder diffraction of the as-synthesized citrate-coated nanoceria.

assess the effect of FaSSGF-exposed nanoceria on Caco-2 cell viability in a medium containing mostly FaSSGF. Caco-2 cell viability was < 5% in 100% FaSSGF and mixtures containing equal volumes of FaSSGF and cell culture medium compared to phosphate- & FBS-free DMEM. Caco-2 cell viability averaged ~10 and 95% in the presence of 90% FeSSGF:10% phosphate-FBS-free DMEM and 75% FeSSGF:25% phosphate-FBS-free DMEM, respectively, compared to phosphate-FBS-free DMEM. Caco-2 cell viability averaged 109 and 97% in the presence of 90% FaSSIF or FeSSIF, respectively:10% phosphate-FBS-free DMEM, compared to phosphate-FBS-free DMEM. Based on these results, during the viability assay Caco-2 cells were exposed to 75% of FeSSGF and 25% phosphate- & FBS-free DMEM, or 90% of the simulated intestinal fluids and 10% phosphate- & FBS-free DMEM. Viability assays were conducted in three independent experiments, each containing two wells with each nanoceria concentration. LPS and Triton-X 100 were tested as positive controls. Two-hour exposure to 0.1, 0.3, or 1 μg/ml LPS reduced Caco-2 cell viability 3, 13, and 11%, respectively. Six-hour exposure to these concentrations reduced Caco-2 cell viability 7, 13, and 13%, respectively. We (unpublished results with RAW 264.7 cells) and others have found LPS effects to be quite concentration independent [73]. Two-hour exposure to 0.001, 0.003, 0.01, 0.03, 0.1, 0.3, 1, 3, or 10% Triton-X 100 reduced Caco-2 cell viability to ~0 for all but the two lowest concentrations (~90% viability). After six-hour exposure to 0.001 and 0.003% Triton-X 100, Caco-2 cell viability was ~80 and 50%, respectively. These results demonstrate resazurin assay sensitivity to reduced cell metabolism.

2.2.7. Assessment of nanoceria effect on cellular respiration before and after SBF exposure

Cellular oxygen consumption rates (OCRs) of A549 and Caco-2 cells in response to uncoated, citrate-coated, and SBF-exposed citrate-coated nanoceria were determined using a Seahorse XFe96 Analyzer (Agilent). The standard Seahorse XF Cell Mito Stress Test protocol was performed by measurement of OCRs after stepwise injection of 2.5 μM oligomycin, FCCP (0.5 μM for A549 cells and 0.25 μM for Caco-2 cells), and 1 μM rotenone and 10 μM Antimycin A that generated multiple endpoints of cellular respiration. A549 cells (25,000/well) were exposed for three h to DMEM with 10% FBS, phosphate-FBS-free DMEM, uncoated and citrate-coated nanoceria in phosphate-FBS-free DMEM, SLF, and nanoceria in SLF that had been immediately previously exposed to SLF for three h. Caco-2 cells (20,000/well) were exposed to the same conditions for two h with FeSSGF replacing SLF and for six h with FaSSIF and FeSSIF replacing SLF. Nanoceria was tested at 0, 1, 5, 20, and 100 μg/cm^2 Seahorse plate well area, equivalent to 0, 1.1, 5.7, 23, and 114 μg/ml. Each condition was tested in at least duplicate wells in at least three replicate experiments.

2.2.8. Data and statistical analysis

Zeta potential results were fitted using a Carreau equation that models "plateau" areas at high and low pH values and a logarithmic region between these two extremes, as we previously employed [74].

The uncoated TGA nanoceria data were used as a control for water loss, and additional weight losses from the coated samples were attributed to organic acids (acetic, citric, maleic, or taurocholic acid) or casein (in the FeSSGF sample). The temperature of comparison was 500 °C. Material balances were calculated on the organic acid weight losses for an average nanoceria particle size (21.1 nm side length, 9393 nm^3 volume). Lost organic coating weights were converted to lost volumes using the densities of the specific organic acids, giving an estimate of the nanoceria + coating volume and cubic diameter. These were compared to the size of an individual organic acid to estimate whether the coating was much less than a monolayer, ¼ to ½ a monolayer, a monolayer, or larger. The FeSSGF sample contained milk proteins, of which 80% are caseins. Caseins are well-known colloidal particle adsorbents and stabilizers [75,76] and proteins are known to adsorb to nanoceria [74]. K-casein, an appropriate model for milk proteins, is known to have a typical area of 40 nm^2 when adsorbed on colloids [75]. The average nanoceria particle had a surface area of 2646 nm^2. If K-casein coverage was a monolayer, the average nanoceria particle of 21.1 nm side length would have 66 K-casein molecules attached to its surface. The weight of the adsorbed layer was then compared directly to the weight of 66 K-casein molecules.

Resazurin assay absorbance in the absence of cells was subtracted from the absorbance from cell metabolism, expressed as a percentage of the latter, and nanoceria concentration dependence, compared to its absence, assessed for statistical significance by one-way ANOVA. Cell viability was determined from the one h absorbance results (absorbance was linear from zero to one to two h). Results are reported as mean ± S.D.

Oxygen consumption rate results were baselined to non-mitochondrial respiratory rates and further normalized to the protein content in the respective well (determined by the BCA method). The effect of phosphate-FBS-free DMEM on cell respiration was determined by comparing the OCR to it and DMEM with 10% FBS. The effect of SBF on cell respiration was determined by comparing cell response to the SBF and phosphate-FBS-free DMEM. The effect of uncoated and citrate-

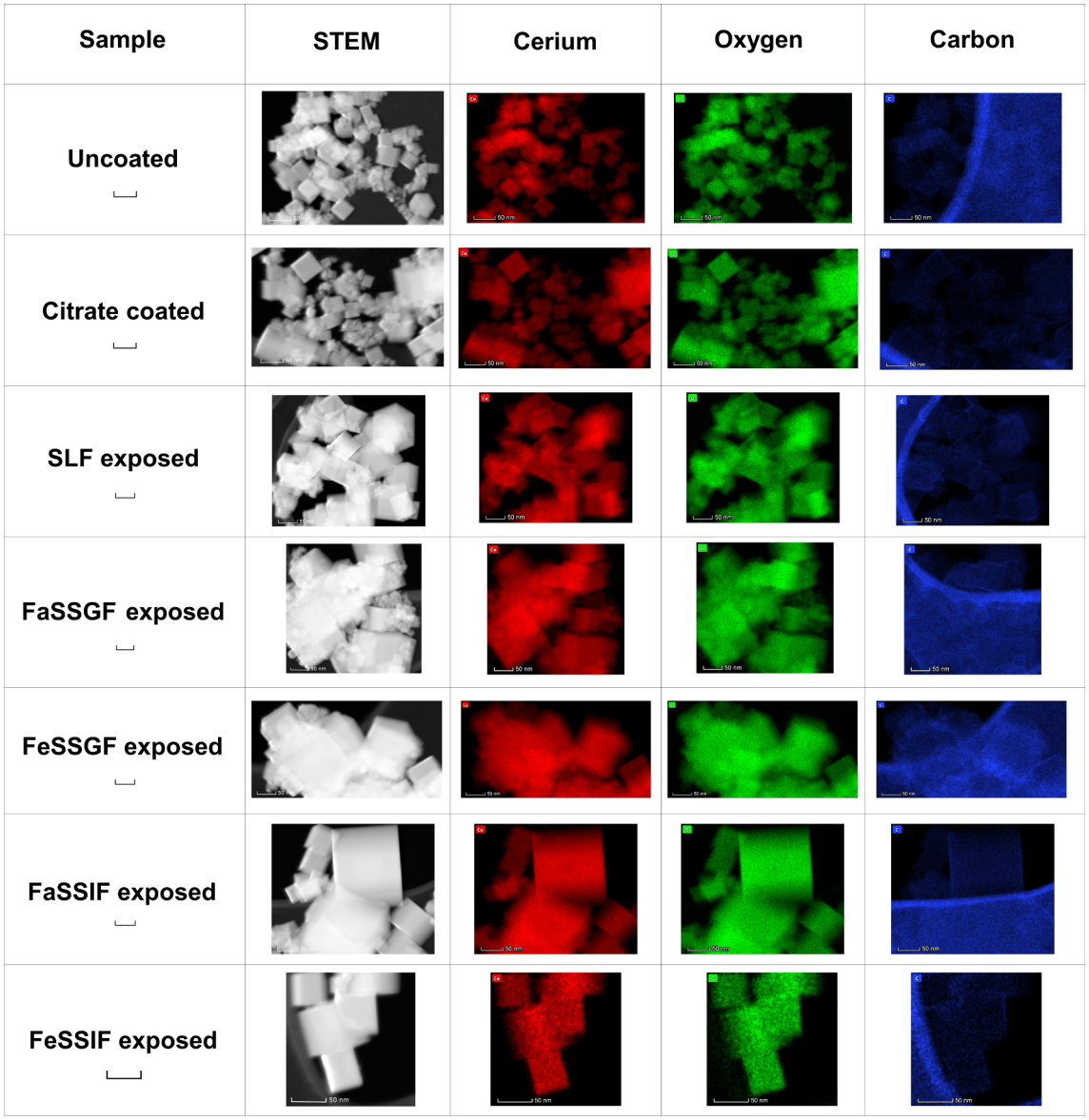

Fig. 2. STEM images of nanoceria before and after SBF exposure and surface cerium, oxygen, and carbon elemental maps. Each of the images in a row are the same size. A 50 nm scale bar is in the first column of the row.

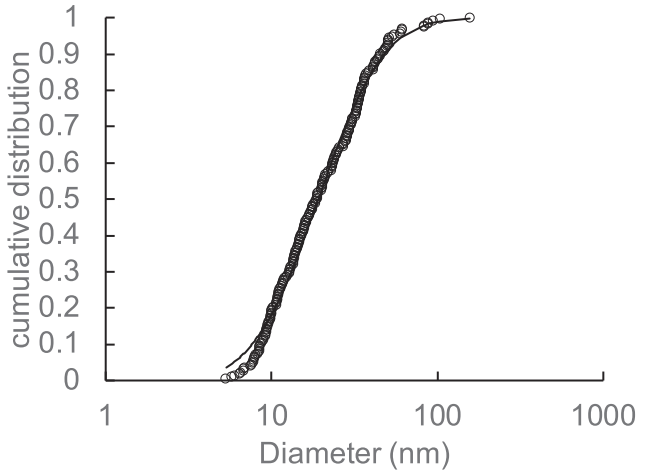

Fig. 3. Primary particle size distribution. Open circles are results of the 231 sized particles. Solid line is the log normal distribution model for best fit.

coated nanoceria on basal and maximal OCR was determined as the response of cells exposed to nanoceria in phosphate-FBS-free DMEM/ cells exposed to phosphate-FBS-free DMEM. The effect of SBF exposed-nanoceria on cellular respiration was determined as the response to SBF- exposed nanoceria in SBF/the SBF. The mean and standard deviation of the experimental averages was calculated and subjected to one-way ANOVA to test for significant differences between nanoceria and non-nanoceria-exposed cells.

3. Results

3.1. Uncoated and citrate-coated nanoceria characterization results

X-ray diffraction analysis and selected area electron diffraction of the uncoated and citrate-coated nanoceria demonstrated its crystallinity and showed (1 1 1), (2 0 0), (2 2 0), and (3 1 1) crystal planes. Fig. 1 shows a representative XRD example for citrate-coated nanoceria and the predominant crystal planes. Consistent results were obtained with selected area electron diffraction (results not shown). The crystalline nature was similar to the reported spectrum for cerium oxide

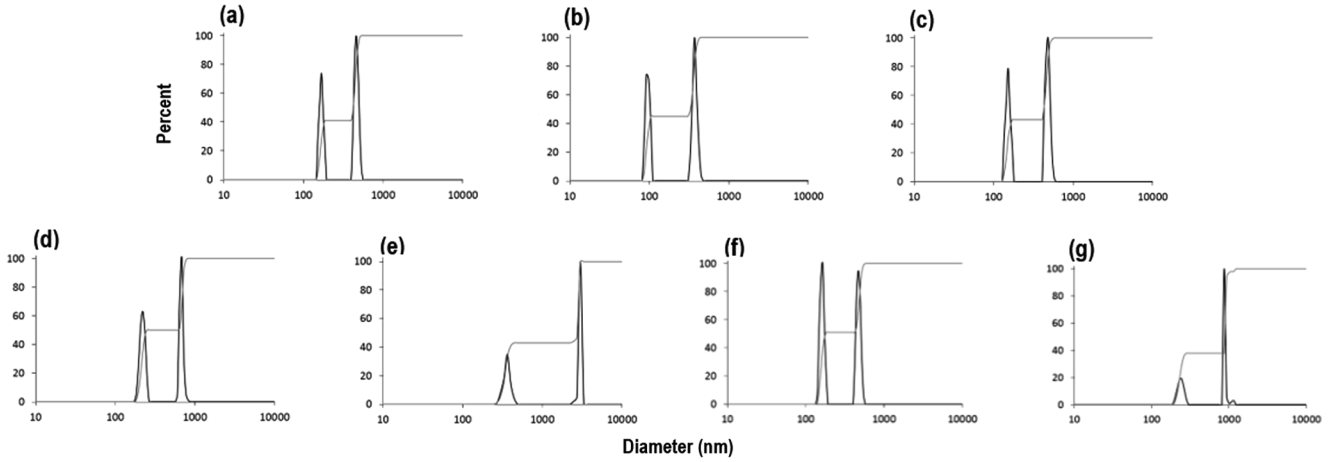

Fig. 4. Nanoceria hydrodynamic diameter, as surface area, before and after SBF exposure. (a) Nanoceria before citrate coating and SBF exposure. (b) Citrate-coated nanoceria before SBF exposure. Nanoceria after exposure to (c) SLF, (d) FaSSGF, (e) FeSSGF, (f) FaSSIF, and (g) FeSSIF.

Table 1
Nanoceria hydrodynamic size.

Nanoceria sample	Bimodal size distribution (% by nm range)
Uncoated	41% 150–180; 59% 415–540
Citrate coated	45% 85–105; 59% 310–450
SLF exposed	43% 135–170; 57% 430–575
FaSSGF exposed	50% 185–250; 50% 600–775
FeSSGF exposed	43% 270–445; 57% 2450–3000
FaSSIF exposed	51% 135–185; 49% 420–550
FeSSIF exposed	38% 185–285; 62% 870–1150

(JCPDS Card #34_0394). The crystal structure of nanoceria is cubic fluorite [77]. STEM images of the uncoated and citrate-coated nanoceria as well as the nanoceria after SBF exposure show it was cubic-shaped (Fig. 2). Primary particle size (particles that cannot be separated into smaller particles except by the application of ultrahigh energy) determined by TEM is shown in Fig. 3. Primary particle size distribution was best described as log normal. The mean (S.D.) particle size was 21.1 (14.2) nm. Hydrodynamic diameter (the apparent size of the solvated/dynamic hydrated particle in an aqueous medium) results determined by DLS, as surface area, are displayed in Fig. 4, and summarized in Table 1. The hydrodynamic diameter of the uncoated and citrate-coated nanoceria was greater than the primary particle diameter determined by TEM, suggesting particle agglomeration. Citrate coating produced an

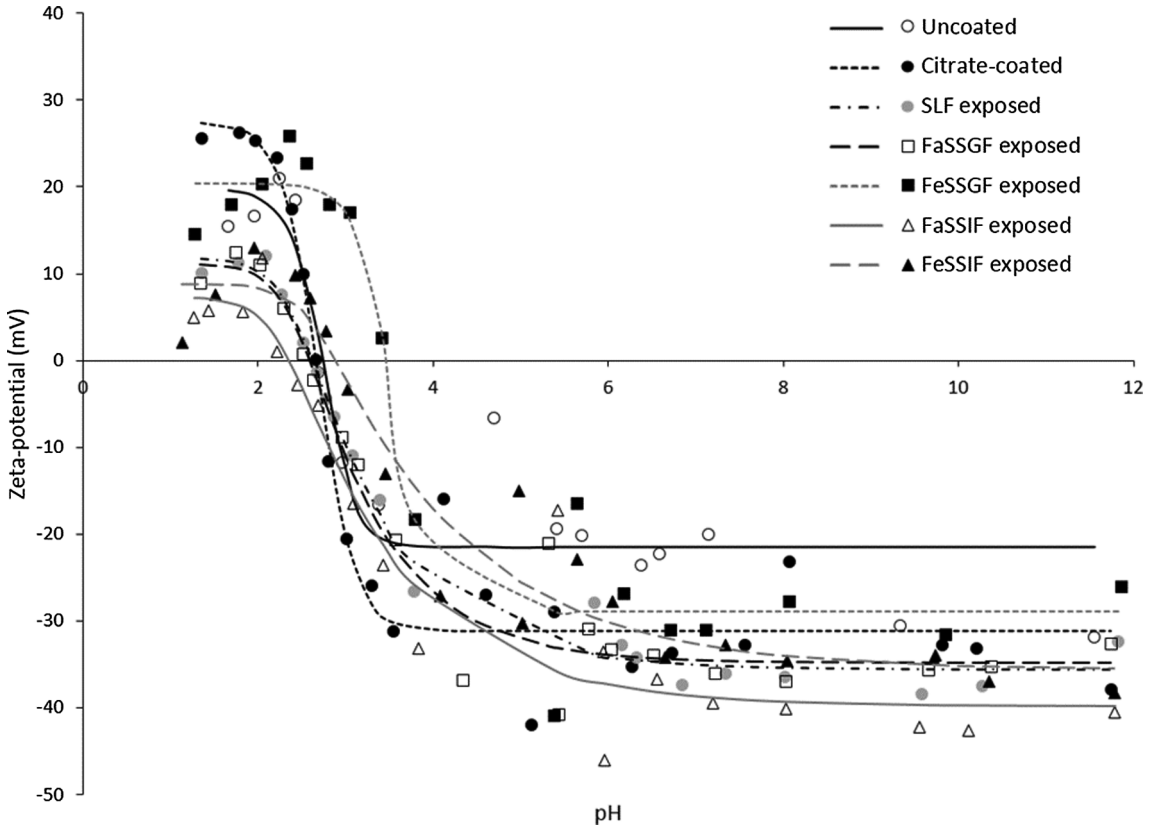

Fig. 5. Nanoceria surface charge (zeta potential) before and after citrate coating, and after exposure to each SBF.

Table 2
Model estimates of the isoelectric point (IEP) and upper (ζ_0) and lower (ζ_{inf}) pH plateau zeta potentials.

	Uncoated	Citrate coated	SLF exposed	FaSSGF exposed	FeSSGF exposed	FaSSIF exposed	FeSSIF exposed
IEP (pH)	2.7	2.7	2.6	2.6	3.5	2.4	2.9
ζ_0 (mV)	19.8	27.5	11.9	11.1	20.4	7.3	8.8
ζ_{inf} (mV)	−21.5	−31.1	−35.6	−34.8	−29.0	−39.8	−35.6

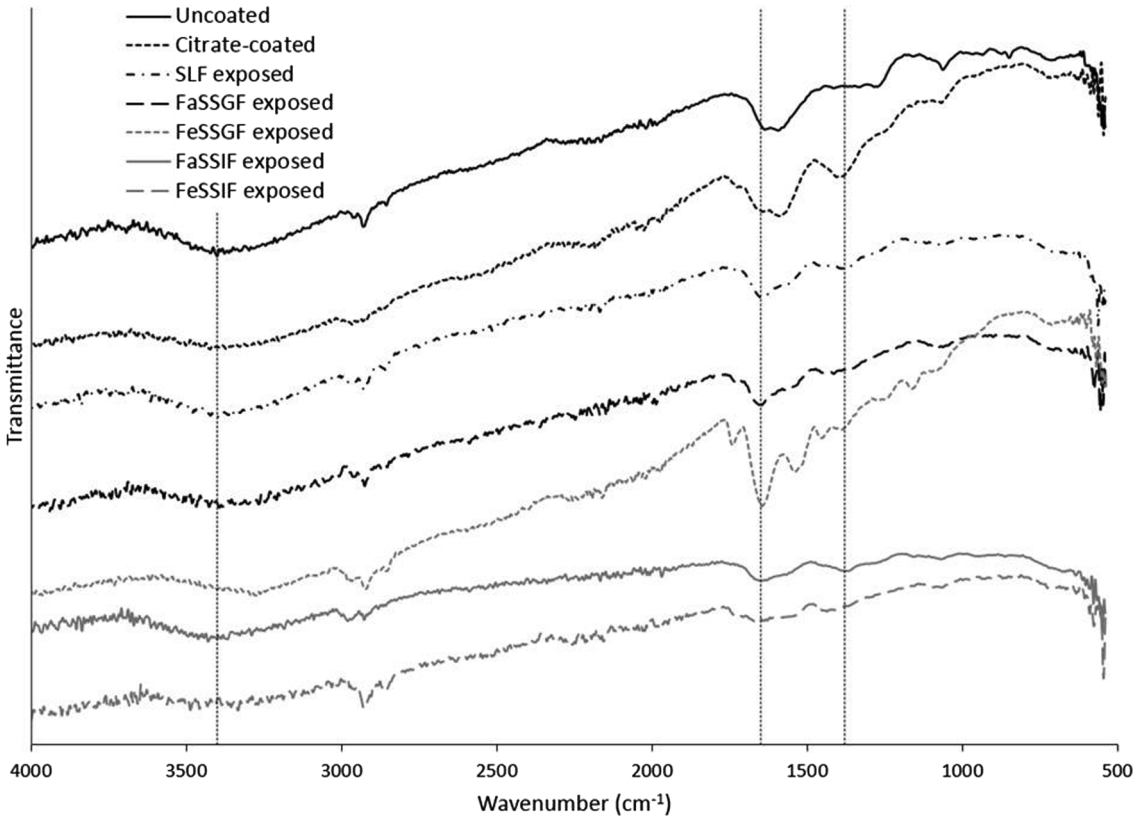

Fig. 6. Fourier transform infrared spectroscopy of the nanoceria before and after citrate coating and after exposure to each SBF. Vertical dashed lines indicate −OH at 3400, N−O at 1650, and −COOH at 1380 cm^{-1}.

Table 3
Estimated coating thickness of citrate and simulated body fluids on nanoceria.

Sample	Sorbed ligand	Diameter of sorbed complex (nm)	Adsorbate molecule diameter (nm)	Coating thickness
Uncoated	Control	21.1	Control	Control
FaSSIF exposed[a]	Maleic acid	21.2	0.61	≪ monolayer
SLF exposed[a]	Acetic acid	21.2	0.57	≪ monolayer
FaSSGF exposed[a]	Taurocholic acid	21.3	1.1	≈¼ monolayer
Citrate coated[a]	Citric acid	21.4	0.72	≈½ monolayer
FeSSIF exposed[a]	Maleic acid	21.6	0.61	≈ 1monolayer
FeSSGF exposed[b]	K-casein	Not applicable	Not applicable	1 to 2 layers

[a] Estimated from the weight of the coating for the average nanoceria particle diameter.
[b] Estimated by assuming that K-casein adsorbed to the average nanoceria particle size and comparing the adsorbed weight to a closely packed (one layer) or randomly packed (two layers) structure.

~10 mV greater absolute (negative) surface charge in the circumneutral pH range (Fig. 5) and a lower (ζinf) pH plateau zeta potential of ~30 mV (Table 2). This was associated with an ~25% reduction of the hydrodynamic diameter, attributed to the greater surface charge-induced repulsion of the like-charged nanoceria particles. Successful surface coating with citric acid is confirmed by FTIR (Fig. 6) that shows an additional peak at (1380 cm^{-1}) attributed to $-COO^-$ symmetric stretch and the 1% greater weight loss during TGA analysis (Fig. 8). This translates to on average 0.8 citrate molecules per nm^2 on the surface of the primary particle that translates to about ½ a monolayer (Table 3). This estimate assumes complete packing of the adsorbate molecules on the surface. Random packing of adsorbates on surfaces often covers only 50 to 54% of the available area [71].

3.1.1. Effect of simulated body fluid (SBF) exposure on citrate-coated nanoceria and effect of non- and SBF-exposed nanoceria on cell viability

Exposure to SBFs for two to six h produced no observable surface degradation (Fig. 2); but SBF-dependent effects on hydrodynamic diameter (Fig. 4 and Table 1), surface carbon (Fig. 2), zeta potential (Fig. 5 and Table 2), FTIR (Figs. 6 and 7), and TGA (Fig. 8) were seen. Citrate-

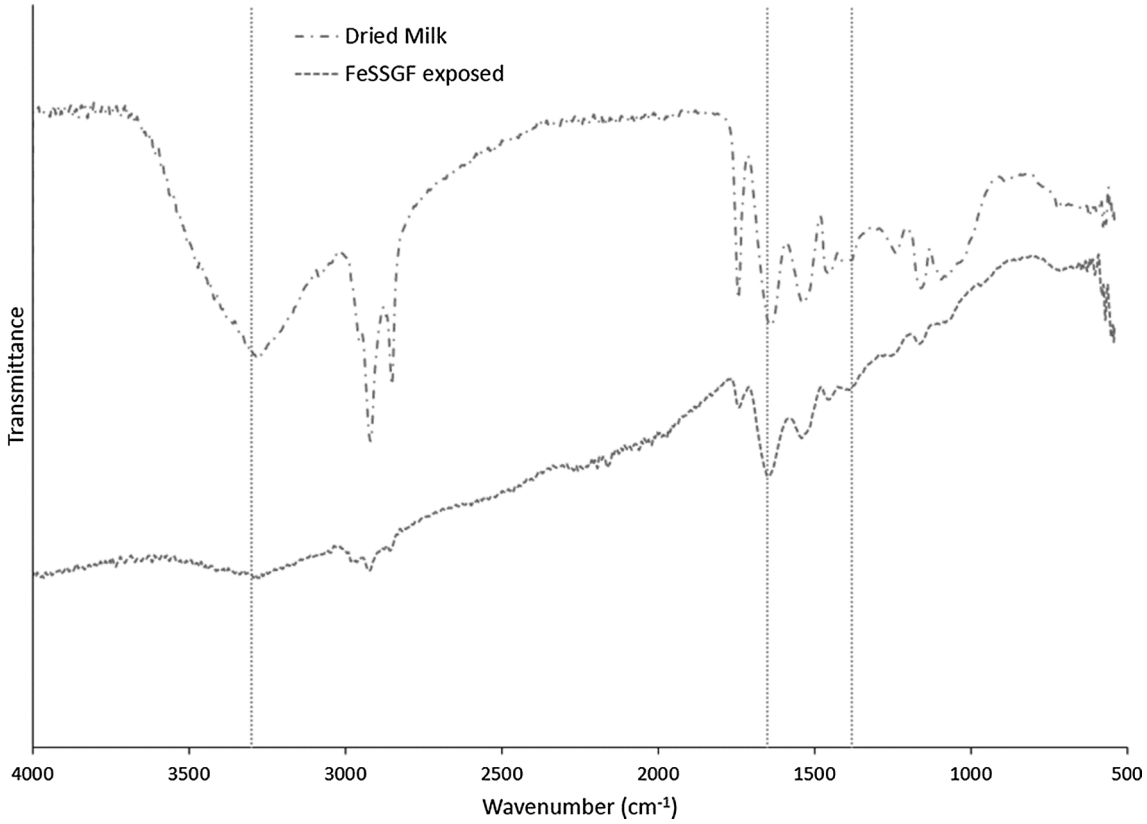

Fig. 7. Fourier transform infrared spectroscopy of dried milk and nanoceria after FeSSGF exposure. Vertical dashed lines indicate −OH at 3300, N−O at 1650, and −COOH at 1380 cm^{-1}.

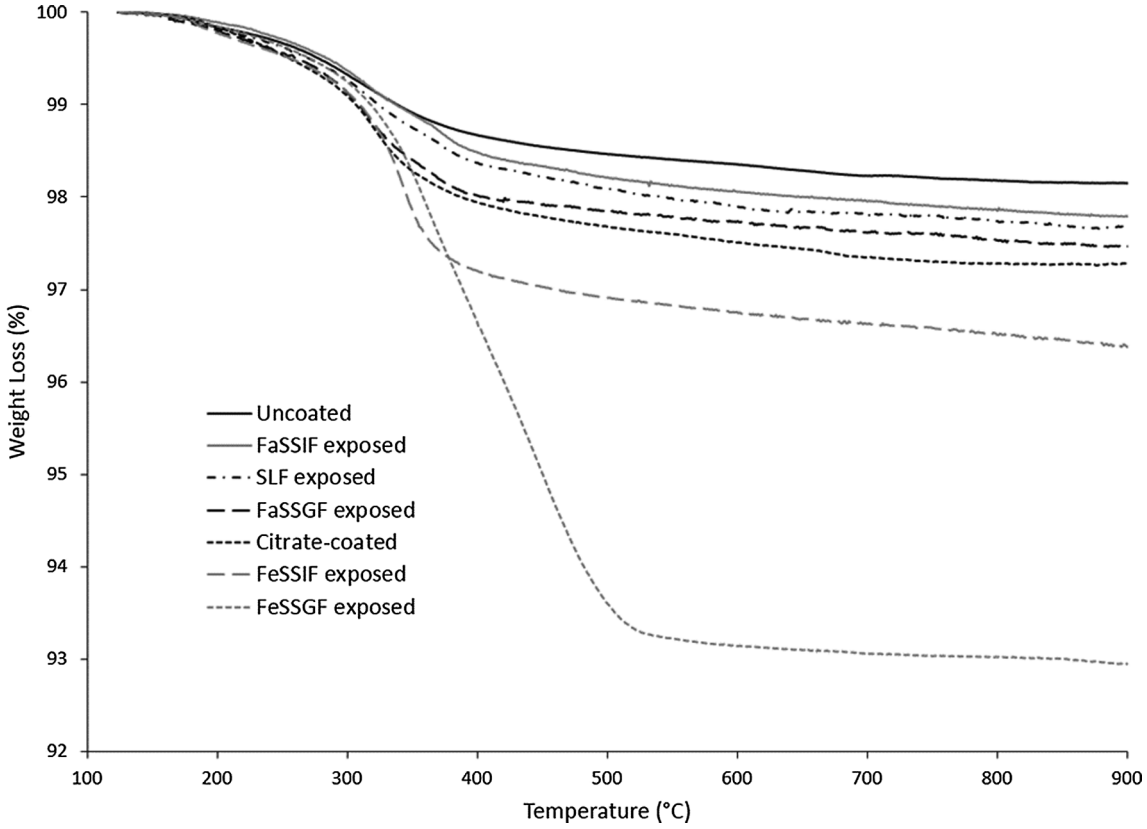

Fig. 8. Thermogravimetric analysis of nanoceria before and after citrate coating, and after exposure to each SBF.

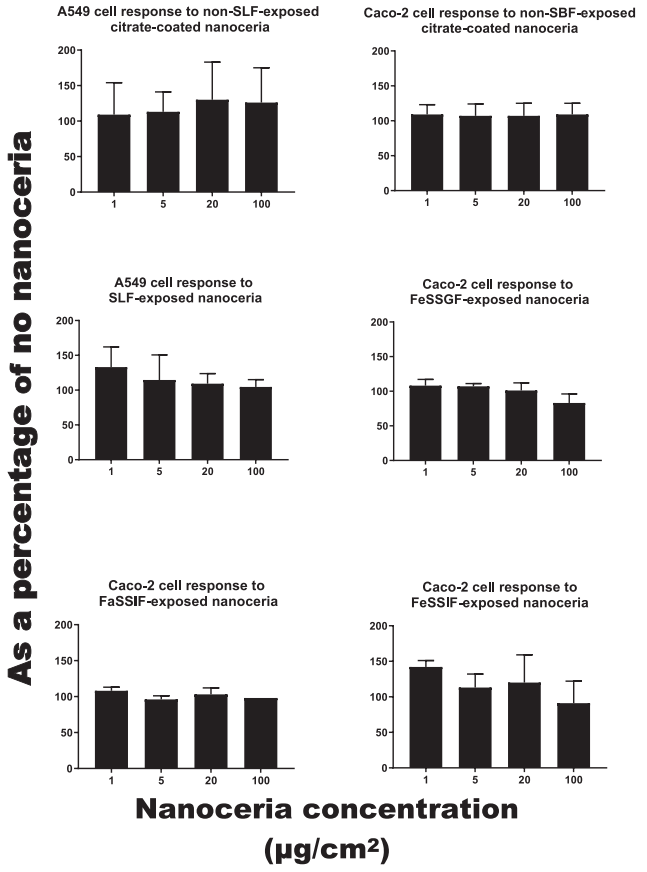

Fig. 9. Cell viability after exposure to nanoceria that had not or had been SBF exposed. The standard deviation of the 100 μg/cm^2 results in the lower left panel "Caco-2 cell response to FaSSIF-exposed nanoceria" is 0.

coated and SBF-exposed nanoceria, up to 100 μg/cm^2, did not significantly affect A549 or Caco-2 cell viability (Fig. 9). Details are described below.

Exposure to SLF resulted in a small increase in the mean hydrodynamic diameter (Fig. 4 and Table 1), loss of the FTIR peak at ~1380 cm^{-1} (Fig. 6), and less weight loss during TGA heating than the citrate-coated nanoceria (Fig. 8). These results suggest some removal of citrate from the nanoceria surface with possible replacement by a small amount of acetic acid resulting in minimal coating thickness (Table 3). This was not accompanied by a less negative surface charge (Fig. 5) as might be anticipated with less citric acid on the surface, suggesting some association of SLF components with the CeO_2 surface. A549 cell metabolism was non-significantly increased by three h exposure to SLF-exposed nanoceria (Fig. 9).

Nanoceria exposure to FaSSGF increased its mean hydrodynamic diameter ~80% (Fig. 4 and Table 1), associated with a less positive zeta potential at the FaSSGF pH (1.6) (Fig. 5), the loss of the FTIR peak at ~1380 cm^{-1} that is attributed to citric acid (Fig. 6), and less weight loss during TGA heating than the citrate-coated nanoceria (Fig. 8). The possible loss of citrate from the nanoceria surface may be due to FaSSGF's very low pH (1.6).

Exposure of nanoceria to FeSSGF greatly increased its mean hydrodynamic diameter (Fig. 4 and Table 1). There was no appreciable effect on the zeta potential other than an increase in the isoelectric point (IEP) (Fig. 5 and Table 2). The reduction of the 1380 cm^{-1} FTIR peak attributed to citrate on the nanoceria surface (Fig. 6), appearance of a peak at 1650 cm^{-1}, and large weight loss increase during heating (Fig. 8) may be due to overcoating by FeSSGF component(s), most likely from the milk. There is an additional FTIR peak at ~1750 cm^{-1} suggesting an organic component of milk was associated with the nanoceria surface. An FTIR scan of dried milk is very similar to the FeSSGF-exposed nanoceria scan in the 1300–2000 cm^{-1} range, consistent with nanoceria surface coating by milk components (Fig. 7). K-casein from milk could form a coating that is one (if tightly packed) or two layers (if randomly or loosely packed) thick (Table 3). The system containing protein does form a protein 'corona' around nanoceria. Elemental scan shows FeSSGF-exposed nanoceria had the most carbon on its surface among the SBF-exposed nanoceria. The increases in hydrodynamic diameter and IEP can be attributed to adsorption of milk components on the nanoceria surface. Caco-2 cell viability was not significantly affected by two h exposure to FeSSGF-exposed nanoceria in 75% FeSSGF:25% phosphate- & FBS-free DMEM (Fig. 9).

Exposure of nanoceria to FaSSIF increased its mean hydrodynamic diameter ~25% (Fig. 4 and Table 1). The zeta potential at the FaSSIF pH (6.5) became ~9 mV more negative (Fig. 5), the 1380 cm^{-1} FTIR peak was greatly reduced (Fig. 6), and weight loss during heating was less than seen with citrate-coated nanoceria (Fig. 8). The considerable loss of the 1380 cm^{-1} FTIR peak attributed to citrate on the nanoceria surface in the absence of increased weight loss during heating and lack of additional FTIR peaks suggests removal of most of nanoceria's surface citrate without significant coating by FaSSIF's organic components (Table 3). FaSSIF-exposed nanoceria in 90% FaSSIF:10% phosphate-FBS-free DMEM had little effect on Caco-2 cell viability (Fig. 9).

Nanoceria exposure to FeSSIF increased its mean hydrodynamic diameter ~155% (Fig. 4 and Table 1). The zeta potential at the FeSSIF pH (5.8) became less negative (Fig. 5), the 1380 cm^{-1} FTIR peak was greatly reduced in the absence of any new peaks (Fig. 6), and there was a considerable increase of the weight loss during heating (Fig. 8). The loss of the 1380 cm^{-1} FTIR peak and increased weight loss during heating suggests overcoating by some FeSSIF component(s), perhaps maleic acid, that would produce a monolayer coat on the nanoceria (Table 3). The lowest concentration (1 μg/cm^2) of FeSSIF-exposed nanoceria in 90% FeSSIF:10% phosphate-FBS-free DMEM non-significantly increased Caco-2 cell viability, whereas higher concentrations had little effect (Fig. 9).

3.1.2. Effect of nanoceria and simulated body fluid (SBF) exposed nanoceria on the oxygen consumption rate

Basal and maximal A549 OCRs in phosphate-FBS-free DMEM were 102 ± 2% (mean ± S.D.) and 102 ± 1% of respiration in DMEM with 10% FBS, respectively. Caco-2 basal and maximal cell respiration after two h were 85 ± 7% and 95 ± 7%, and after six h 93 ± 3% and 97 ± 3% in phosphate-FBS-free DMEM compared to DMEM with 10% FBS. A549 basal and maximal cell respiration in SLF were 91 ± 9% and 93 ± 10% compared to phosphate-FBS-free DMEM. Caco-2 basal and maximal cell respiration in FeSSGF, FaSSIF, and FeSSIF were 94 ± 25% and 88 ± 36%, 82 ± 13% and 87 ± 6%, and 84 ± 15% and 67 ± 12% compared to phosphate-FBS-free DMEM, respectively.

Fig. 10 shows a representative trace for A549 and Caco-2 results, indicating that the cell respiration analyses were performing correctly, and responsive to treatments (oligomycin, FCCP, rotenone and antimycin A, and cell culture media). Fig. 11 shows the effects of uncoated, citrate-coated, and SBF-exposed nanoceria on cellular respiration. There were no statistically significant differences between nanoceria treatments and the control (nanoceria free) condition. The results suggest nanoceria, uncoated, coated, or SBF-exposed, does not have a profound effect on A549 or Caco-2 cell respiration up to 100 μg/cm^2 (114 μg/ml), a quite high concentration.

4. Discussion

To our knowledge this is the first study to investigate the corona formed on nanoceria after exposure to GI fluids and the effects of lung and GI fluid corona on cell response.

The lack of change in nanoceria primary particle size or shape during its two to six h SBF exposure was expected, given its slow

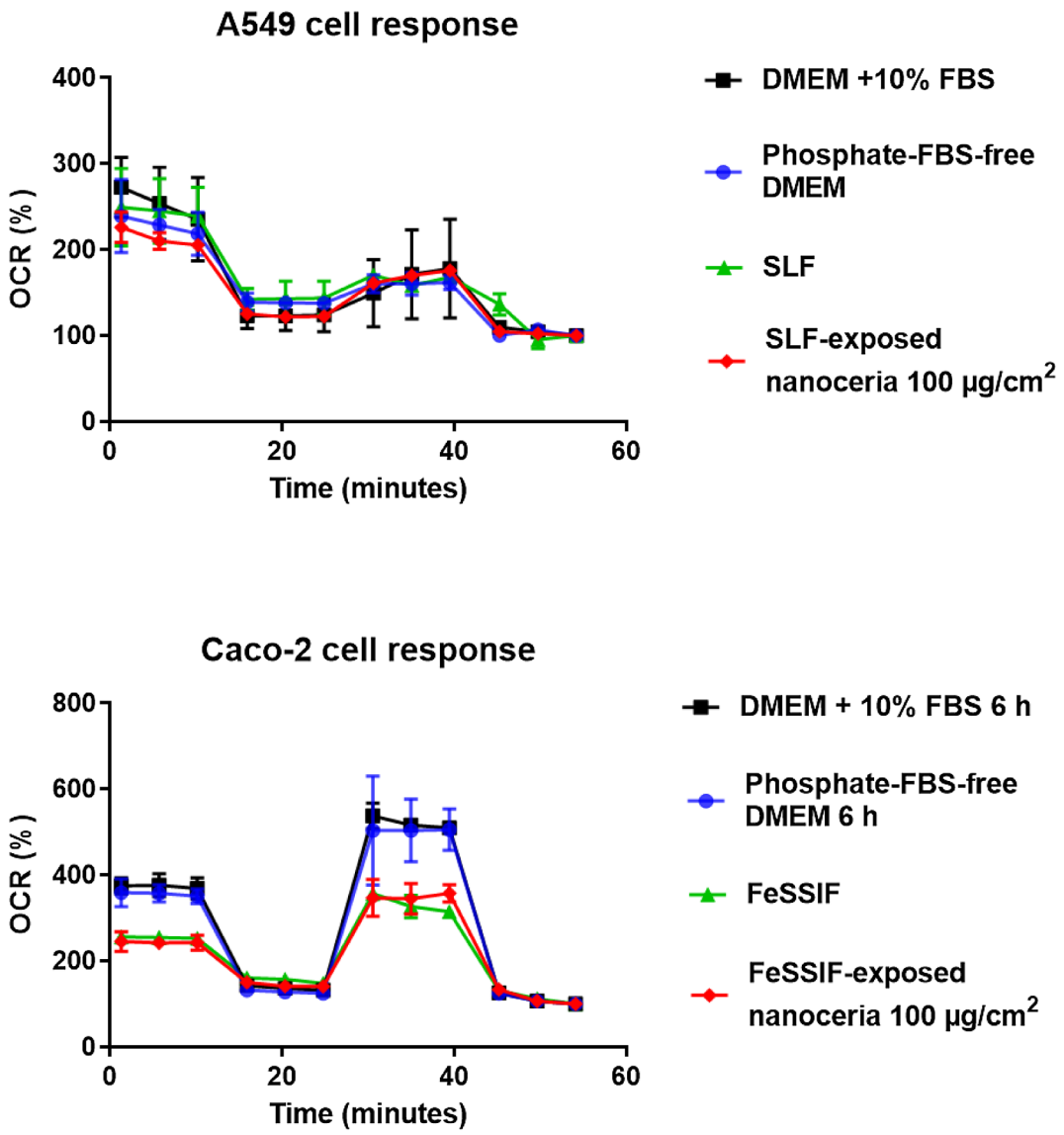

Fig. 10. A549 and Caco-2 cell oxygen consumption rate response to selected media and SBF-exposed nanoceria. Upper panel: A549 cell OCR response to selected media and 100 µg/cm^2 SLF-exposed nanoceria. Lower panel: Caco-2 cell OCR response to selected media and 100 µg/cm^2 FeSSIF-exposed nanoceria.

solubility at acidic pH, and lack of significant solubility at circumneutral pH [17,78,79] and prior studies cited in the introduction to Yokel et al, 2019 [79].

Although there are many reports of nanoceria zeta potential, few provide sufficient details, such as pH and medium, to fully interpret the results. Even fewer determined the zeta potential as a function of pH, as conducted in this study. Two studies reported nanoceria from commercial sources to have an IEP of ~pH 7 in water [80,81], very different from the IEPs of our citrate-coated nanoceria. The surface properties of these commercial materials are unknown. We have unpublished results that show nanoceria annealed at 300 °C for one h has an IEP of 7.

The increase in nanoceria's absolute (negative) surface pH after exposure to SLF is probably due to association of phosphate with the surface Ce. Cerium is known to form a complex with phosphate [82]. Cerium phosphate is quite insoluble, with reported log stability/formation/equilibrium constants for Ce^{3+} phosphate of 3.4×10^{18} [83] and 3.7×10^{23} [84] and for Ce^{4+} phosphate of 2.9×10^{34} [85].

Some prior studies of A549 viability found no significant effect after four or more h nanoceria exposure up to or beyond 100 µg/ml [86–90]. In contrast, a significant decrease after 24 h exposure to 3.5 µg/ml nanoceria [91], ~ 90% viability three h after 33 µg/ml [92], 80 and 86% viability six and 24 h after exposure to 195 µg/ml [93], 90 and 85% viability after 24 h exposure to 100 and 1000 µg/ml [64], and a 10 to 20% viability reduction after 24 h exposure to 67 µg/ml [94] were reported. In contrast to a reduction of viability, increased cell viability after 24 h exposure to five to 40 µg/ml of 50 and 300 (but not 30) nm ceria was reported [95]. The lack of decreased A549 viability in the present study after three h exposure to up to 100 µg/cm^2 citrate-coated nanoceria agrees with most prior reports. Exposure to SLF (Gamble's solution) did not significantly affect nanoceria toxicity. Similar to most studies with A549 cells, prior studies found no effect on Caco-2 cell viability after 24 h exposure to up to 200 µg/ml nanoceria [89,96]. Results of the present study with SBF-exposed nanoceria are similar, however they suggest that exposure to $>$ 100 µg/cm^2 fed-state gastric or intestinal fluid might significantly reduce Caco-2 cell viability. In contrast, Caco-2 cell metabolism was reduced when exposed to $<$ 100 µg/ml SBF-exposed silver NPs [4], 100 µg/ml FaSSIF-exposed silica NPs [8], $<$ 100 µg/cm^2 SBF-exposed silica or ZnO NPs [9], and 10 µg/ml SBF-exposed nanotitania [12]. Rat IEC-6 cell metabolism was reduced when exposed to $<$ 100 µg/ml CuO NPs [10].

Similar to the cell viability response of A549 and Caco-2 cells to coated and SBF-exposed nanoceria, OCR was not significantly affected

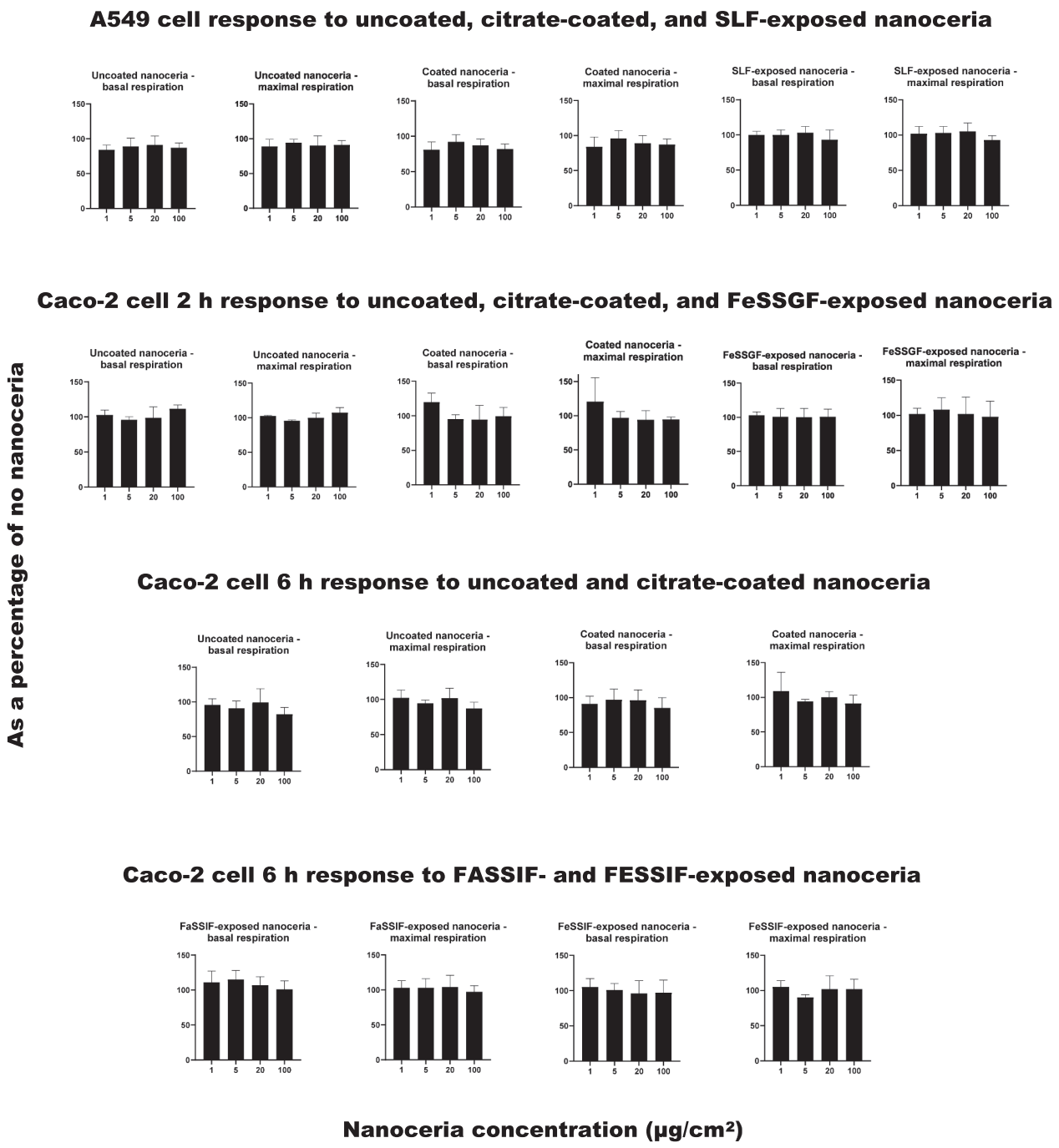

Fig. 11. A549 and Caco-2 cell basal and maximal oxygen consumption rate responses to uncoated, citrate-coated, and SBF-exposed nanoceria.

by uncoated, coated, or SBF-exposed nanoceria. There are no prior reports of OCR response to nanoceria. A549 and undifferentiated Caco-2 cell OCR were shown to be responsive to nanomaterial and chemical insult [97,98].

The lack of considerable effect of nanoceria on resazurin metabolism and OCR may be partly due to the physical incompatibility of nanoceria in the SBFs. Introduction of the citrate-coated nanoceria (as an aqueous dispersion) as well as the nanoceria that had been exposed to SBFs (that were dispersed in the SBFs), resulted in visually noticeable nanoceria precipitation on the cells. This indicates the lack of stability of nanoceria in the SBFs, which would be expected to reduce its potential for cell uptake or cell membrane effects. This may contribute to the low biological effects of citrate-coated nanoceria (adverse or beneficial) before and after SBF exposure.

Nanoceria has been shown to be taken up by A549 and Caco-2 cells. Nanoceria (9 nm) was observed by TEM in A549 cell vesicular structures and cytoplasm within 10 min of exposure. Using ICP-MS to study uptake kinetics revealed non-saturated, ~ linear cell association of ~60% of the nanoceria after 30 min [56]. Four h after exposure TEM showed 8 and 20 nm ceria close to the A549 cell surface and in aggregates in endocytotic vacuoles. Uptake was concentration dependent (from 10, 50, and 200 μg/ml) for 24 h [87]. Confocal microscopy of Caco-2 cells showed nanoceria particles in fully differentiated (grown for 14 days) Caco-2 cells after 24 h exposure to 3.125 and 31.25 mg/cm^2 < 25 nm ceria [99], and in undifferentiated Caco-2 cells, including the nucleus, after 24 h exposure to 100 μg/ml 70 nm ceria [96].

Nanoceria concentrations in the present study that did not produce significant effects on A549 cells (≥1 μg/cm^2) are greater than the

nanoceria concentration in ambient air attributed to use of nanoceria in diesel fuel (0.5 ng/m^3) [100]. The only published study we are aware of that assessed occupational nanoceria exposure did not find cerium in air samples during chemical mechanical planarization in semiconductor device fabrication [101]. A two-year study of nanoceria inhalation (NM-212, 40 nm, agglomerates three to 150 μm) was conducted in rats exposed to 0.1, 0.3, 1, or 3 mg/m^3, 6 h daily, 5 days weekly. This resulted in time- and dose-dependent increased polymorphonuclear leukocytes in the bronchoalveolar lavage fluid (indicating inflammation), granuloma formation and giant cells after 12 months exposure to 1 mg/m^3, and moderate chronic inflammation after 24 month exposure to 3 mg/m^3 [102]. An aerosol containing 1 mg/m^3 nanoceria would contain one μg in 1000 cm^3. Rat minute ventilation is ~30 mL(cm^3)/min [103]. One μg/cm^2 (the lowest A549 cell exposure of the present study) would represent the nanoceria inhaled from 1 mg/m^3 by a rat in ~0.5 h. The A549 results suggest neither the citrate-coated or SLF-exposed nanoceria would be predicted to result in adverse effects after acute exposure to the nanoceria concentrations studied in rats or likely to be inhaled by humans during occupational exposure.

5. Conclusion

Nanoceria synthesis was confirmed by XRD and selected area electron diffraction results (crystalline identity) and EDS results (cerium and oxygen). Citrate coating addition was demonstrated by a decrease in hydrodynamic diameter, an increase in the absolute surface charge, FT-IR appearance of a carboxylate-assignable peak, and a moderate increase in mass loss during TGA heating. Some of the citrate persisted on the nanoceria surface after SBF exposure. Following FeSSGF exposure, hydrodynamic diameter and weight loss during heating increased, suggesting addition of material to the nanoceria surface. Similar, but less profound, changes were seen following FeSSIF exposure. Exposure to SLF, FaSSGF, and FaSSIF resulted in subtle changes. Neither the citrate-coated or SBF-exposed nanoceria produced significant cell toxicity, suggesting acute nanoceria exposure to concentrations less than extraordinary would not be predicted to produce adverse pulmonary or gastrointestinal effects.

Acknowledgements

This work was supported by the National Science Foundation REU Program #EEC-1460486 and the National Institutes of Health [grant number R01GM109195]. The content is solely the responsibility of the authors and does not necessarily represent the official views of the National Institutes of Health. The authors thank the following for their instruction and assistance: Andrew Colburn: zeta potential measurements, Soledad Yao: FT-IR; Nancy Miller: XRD; and Dr. Dali Qian: TEM.

Declaration of Competing Interest

The authors declare that they have no competing interests.

Author contributions

RAY conceived and coordinated the study, wrote drafts of the report, and coordinated report input from the authors. BC contributed to this work as a summer research student at the University of Kentucky. BC and AJB synthesized nanoceria and conducted initial studies of SBF-exposed nanoceria, that were followed up by MLH. MLH synthesized the nanoceria and conducted most of the nanoceria SBF exposures. EAG provided input on the nanoceria synthesis, purification, and SBF exposure; oversaw EM imaging; and conducted primary particle size determination and particle coating thickness estimations. MLE conducted the resazurin assays. HV conducted the Seahorse assays and result calculations. PS guided the interpretation of the Seahorse assay results. All authors approved the revised version of this report.

References

[1] M.P. Monopoli, D. Walczyk, A. Campbell, G. Elia, I. Lynch, F.B. Bombelli, K.A. Dawson, Physical-chemical aspects of protein corona: relevance to *in vitro* and *in vivo* biological impacts of nanoparticles, J. Am. Chem. Soc. 133 (8) (2011) 2525–2534, https://doi.org/10.1021/ja107583h.

[2] E. Casals, M.F. Gusta, V. Puntes, J. Piella, V. Puntes, G. Casals, W. Jimenez, W. Jimenez, V. Puntes, Intrinsic and extrinsic properties affecting innate immune responses to nanoparticles: The case of cerium oxide, Front. Immunol. 8 (2017), https://doi.org/10.3389/fimmu.2017.00970 970/1-970/7.

[3] A.P. Walczak, R. Fokkink, R. Peters, P. Tromp, Z.E. Herrera Rivera, I.M.C.M. Rietjens, P.J.M. Hendriksen, H. Bouwmeester, Behaviour of silver nanoparticles and silver ions in an *in vitro* human gastrointestinal digestion model, Nanotoxicology 7 (7) (2013) 1198–1210, https://doi.org/10.3109/17435390.2012.726382.

[4] L. Böhmert, M. Girod, U. Hansen, R. Maul, P. Knappe, B. Niemann, S.M. Weidner, A.F. Thünemann, A. Lampen, Analytically monitored digestion of silver nanoparticles and their toxicity on human intestinal cells, Nanotoxicology 8 (6) (2014) 631–642, https://doi.org/10.3109/17435390.2013.815284.

[5] A.P. Ault, D.I. Stark, J.L. Axson, J.N. Keeney, A.D. Maynard, I.L. Bergin, M.A. Philbert, Protein corona-induced modification of silver nanoparticle aggregation in simulated gastric fluid, Environ. Sci.: Nano 3 (6) (2016) 1510–1520, https://doi.org/10.1039/C6EN00278A.

[6] C. Kästner, D. Lichtenstein, A. Lampen, A.F. Thünemann, Monitoring the fate of small silver nanoparticles during artificial digestion, Colloids Surf., A 526 (2017) 76–81, https://doi.org/10.1016/j.colsurfa.2016.08.013.

[7] R. Peters, E. Kramer, A.G. Oomen, Z.E. Herrera Rivera, G. Oegema, P.C. Tromp, R. Fokkink, A. Rietveld, H.J.P. Marvin, S. Weigel, A.A.C.M. Peijnenburg, H. Bouwmeester, Presence of nano-sized silica during *in vitro* digestion of foods containing silica as a food additive, ACS Nano 6 (3) (2012) 2441–2451, https://doi.org/10.1021/nn204728k.

[8] K. Sakai-Kato, M. Hidaka, K. Un, T. Kawanishi, H. Okuda, Physicochemical properties and in vitro intestinal permeability properties and intestinal cell toxicity of silica particles, performed in simulated gastrointestinal fluids, Biochim. Biophys. Acta General Subj. 1840 (3) (2014) 1171–1180, https://doi.org/10.1016/j.bbagen.2013.12.014.

[9] K. Gerloff, D.I.A. Pereira, N. Faria, A.W. Boots, J. Kolling, I. Förster, C. Albrecht, J.J. Powell, R.P.F. Schins, Influence of simulated gastrointestinal conditions on particle-induced cytotoxicity and interleukin-8 regulation in differentiated and undifferentiated Caco-2 cells, Nanotoxicology 7 (4) (2013) 353–366, https://doi.org/10.3109/17435390.2012.662249.

[10] T.E. Henson, J. Navratilova, A.H. Tennant, K.D. Bradham, K.R. Rogers, M.F. Hughes, *In vitro* intestinal toxicity of copper oxide nanoparticles in rat and human cell models, Nanotoxicology 13 (6) (2019) 795–811, https://doi.org/10.1080/17435390.2019.1578428.

[11] H. Sieg, C. Kästner, B. Krause, T. Meyer, A. Burel, L. Böhmert, D. Lichtenstein, H. Jungnickel, J. Tentschert, P. Laux, A. Braeuning, I. Estrela-Lopis, F. Gauffre, V. Fessard, J. Meijer, A. Luch, A.F. Thünemann, A. Lampen, Impact of an artificial digestion procedure on aluminum-containing nanomaterials, Langmuir 33 (40) (2017) 10726–10735, https://doi.org/10.1021/acs.langmuir.7b02729.

[12] C. McCracken, A. Zane, D.A. Knight, P.K. Dutta, W.J. Waldman, Minimal intestinal epithelial cell toxicity in response to short- and long-term food-relevant inorganic nanoparticle exposure, Chem. Res. Toxicol. 26 (10) (2013) 1514–1525, https://doi.org/10.1021/tx400231u.

[13] D. Di Silvio, N. Rigby, B. Bajka, A. Mackie, F. Baldelli Bombelli, Effect of protein corona magnetite nanoparticles derived from bread *in vitro* digestion on Caco-2 cells morphology and uptake, Int. J. Biochem. Cell Biol. 75 (2016) 212–222, https://doi.org/10.1016/j.biocel.2015.10.019.

[14] P.N. Wiecinski, K.M. Metz, A.N. Mangham, K.H. Jacobson, R.J. Hamers, J.A. Pedersen, Gastrointestinal biodurability of engineered nanoparticles: development of an *in vitro* assay, Nanotoxicology 3 (3) (2009) 202–214, https://doi.org/10.1080/17435390902859556.

[15] J. Mejia, O. Toussaint, B. Masereel, S. Lucas, Fate of SiC and TiC nanoparticle dispersions in human reconstituted gastric fluid, Int. J. Nano Biomater. 4 (3/4) (2012) 243–255, https://doi.org/10.1504/IJNBM.2012.051706.

[16] É. Pérez-Esteve, M. Ruiz-Rico, C. de la Torre, E. Llorca, F. Sancenon, M.D. Marcos, P. Amorós, C. Guillem, R. MartÍnez-Máñez, J.M. Barat, Stability of different mesoporous silica particles during an *in vitro* digestion, Micropor. Mesopor. Mater. 230 (2016) 196–207, https://doi.org/10.1016/j.micromeso.2016.05.004.

[17] L. Zhong, Y. Yu, H.-Z. Lian, X. Hu, H. Fu, Y.-J. Chen, Solubility of nano-sized metal oxides evaluated by using in vitro simulated lung and gastrointestinal fluids: implication for health risks, J. Nanopart. Res. 19 (11) (2017) 1–10, https://doi.org/10.1007/s11051-017-4064-7.

[18] N.V. Konduru, R.M. Molina, A. Swami, F. Damiani, G. Pyrgiotakis, P. Lin, P. Andreozzi, T.C. Donaghey, P. Demokritou, S. Krol, W. Kreyling, J.D. Brain, Protein corona: implications for nanoparticle interactions with pulmonary cells, Part. Fibre Toxicol. 14 (2017) 42/1-42/12, https://doi.org/10.1186/s12989-017-0223-3.

[19] E. Grulke, K. Reed, M. Beck, X. Huang, A. Cormack, S. Seal, Nanoceria: factors affecting its pro- and anti- oxidant properties, Environ. Sci.: Nano 1 (5) (2014) 429–444, https://doi.org/10.1039/C4EN00105B.

[20] A. Dhall, W. Self, Cerium oxide nanoparticles: a brief review of their synthesis methods and biomedical applications, Antioxidants 7 (8) (2018) 97/1-97/13, https://doi.org/10.3390/antiox7080097.

[21] J. Niu, A. Azfer, L.M. Rogers, X. Wang, P.E. Kolattukudy, Cardioprotective effects

of cerium oxide nanoparticles in a transgenic murine model of cardiomyopathy, Cardiovasc. Res. 73 (3) (2007) 549–559, https://doi.org/10.1016/j.cardiores.2006.11.031.
[22] M.B. Kolli, The use of cerium oxide and curcumin nanoparticles as therapeutic agents for the treatment of ventricular hypertrophy following pulmonary arterial hypertension, Marshall Univ, 2012, p. 147.
[23] S.S. El Shaer, T.A. Salaheldin, N.M. Saied, S.M. Abdelazim, *In vivo* ameliorative effect of cerium oxide nanoparticles in isoproterenol-induced cardiac toxicity, Exp. Toxicol. Pathol. 69 (7) (2017) 435–441, https://doi.org/10.1016/j.etp.2017.03.001.
[24] S. Giri, A. Karakoti, R.P. Graham, J.L. Maguire, C.M. Reilly, S. Seal, R. Rattan, V. Shridhar, Nanoceria: a rare-earth nanoparticle as a novel anti-angiogenic therapeutic agent in ovarian cancer, PLoS ONE 8 (2013) e54578, https://doi.org/10.1371/journal.pone.0054578.
[25] M.S. Wason, J. Colon, S. Das, S. Seal, J. Turkson, J. Zhao, C.H. Baker, Sensitization of pancreatic cancer cells to radiation by cerium oxide nanoparticle-induced ROS production, Nanomedicine 9 (2013) 558–569, https://doi.org/10.1016/j.nano.2012.10.010.
[26] C.K. Kim, T. Kim, I.-Y. Choi, M. Soh, D. Kim, Y.-J. Kim, H. Jang, H.-S. Yang, J.Y. Kim, H.-K. Park, S.P. Park, S. Park, T. Yu, B.-W. Yoon, S.-H. Lee, T. Hyeon, Ceria nanoparticles that can protect against ischemic stroke, Angew. Chem. Int. Ed. 51 (2012) 11039–11043, https://doi.org/10.1002/anie.201207798.
[27] L.L. Wong, J.F. McGinnis, Nanoceria as bona fide catalytic antioxidants in medicine: what we know and what we want to know Adv, Exp. Med. Biol. 801 (2014) 821–828, https://doi.org/10.1007/978-1-4614-3209-8_103.
[28] V. Selvaraj, N. Nepal, S. Rogers, N.D.P.K. Manne, R. Arvapalli, K.M. Rice, S. Asano, E. Fankhanel, J.J. Ma, T. Shokuhfar, M. Maheshwari, E.R. Blough, Inhibition of MAP kinase/NF-kB mediated signaling and attenuation of lipopolysaccharide induced severe sepsis by cerium oxide nanoparticles, Biomaterials 59 (2015) 160–171, https://doi.org/10.1016/j.biomaterials.2015.04.025.
[29] A. Arya, N.K. Sethy, S.K. Singh, M. Das, K. Bhargava, Cerium oxide nanoparticles protect rodent lungs from hypobaric hypoxia-induced oxidative stress and inflammation, Int. J. Nanomed. 8 (2013) 4507–4520, https://doi.org/10.2147/IJN.S53032.
[30] S. Chigurupati, M.R. Mughal, E. Okun, S. Das, A. Kumar, M. McCaffery, S. Seal, M.P. Mattson, Effects of cerium oxide nanoparticles on the growth of keratinocytes, fibroblasts and vascular endothelial cells in cutaneous wound healing, Biomaterials 34 (2013) 2194–2201, https://doi.org/10.1016/j.biomaterials.2012.11.061.
[31] V.C. Minarchick, P.A. Stapleton, T.R. Nurkiewicz, E.M. Sabolsky, Cerium dioxide nanoparticle exposure improves microvascular dysfunction and reduces oxidative stress in spontaneously hypertensive rats, Front. Physiol. 6 (2015), https://doi.org/10.3389/fphys.2015.00339.
[32] N.Y. Spivak, N.D. Nosenko, N.M. Zholobak, A.B. Shcherbakov, A.G. Reznikov, O.S. Ivanova, V.K. Ivanov, Y.D. Tretyakov, The nanocrystalline cerium dioxide raises the functional activity of genesial system of ageing males of rats, Nanosyst.: Phys, Chem, Math. 4 (1) (2013) 72–77.
[33] T. Artimani, I. Amiri, A.S. Soleimani, M. Saidijam, S. Afshar, D. Hasanvand, Amelioration of diabetes-induced testicular and sperm damage in rats by cerium oxide nanoparticle treatment, Andrologia 50 (9) (2018) e13089, https://doi.org/10.1111/and.13089.
[34] R.A. Madero-Visbal, B.E. Alvarado, J.F. Colon, C.H. Baker, M.S. Wason, B. Isley, S. Seal, C.M. Lee, S. Das, R. Manon, Harnessing nanoparticles to improve toxicity after head and neck radiation, Nanomedicine 8 (2012) 1223–1231, https://doi.org/10.1016/j.nano.2011.12.011.
[35] J. Colon, L. Herrera, J. Smith, S. Patil, C. Komanski, P. Kupelian, S. Seal, D.W. Jenkins, C.H. Baker, Protection from radiation-induced pneumonitis using cerium oxide nanoparticles, Nanomedicine 5 (2) (2009) 225–231, https://doi.org/10.1016/j.nano.2008.10.003.
[36] J. Colon, N. Hsieh, A. Ferguson, P. Kupelian, S. Seal, D.W. Jenkins, C.H. Baker, Cerium oxide nanoparticles protect gastrointestinal epithelium from radiation-induced damage by reduction of reactive oxygen species and upregulation of superoxide dismutase 2, Nanomedicine 6 (5) (2010) 698–705, https://doi.org/10.1016/j.nano.2010.01.010.
[37] A.L. Popov, S.I. Zaichkina, N.R. Popova, O.M. Rozanova, S.P. Romanchenko, O.S. Ivanova, A.A. Smirnov, E.V. Mironova, I.I. Selezneva, V.K. Ivanov, Radioprotective effects of ultra-small citrate-stabilized cerium oxide nanoparticles *in vitro* and *in vivo*, RSC Adv. 6 (108) (2016) 106141–106149, https://doi.org/10.1039/C6RA18566E.
[38] K. Chaudhury, K.N. Babu, A.K. Singh, S. Das, A. Kumar, S. Seal, Mitigation of endometriosis using regenerative cerium oxide nanoparticles, Nanomedicine 9 (2013) 439–448, https://doi.org/10.1016/j.nano.2012.08.001.
[39] K.L. Heckman, W. DeCoteau, A. Estevez, K.J. Reed, W. Costanzo, D. Sanford, J.C. Leiter, J. Clauss, K. Knapp, C. Gomez, P. Mullen, E. Rathbun, K. Prime, J. Marini, J. Patchefsky, A.S. Patchefsky, R.K. Hailstone, J.S. Erlichman, Custom cerium oxide nanoparticles protect against a free radical mediated autoimmune degenerative disease in the brain, ACS Nano 7 (12) (2013) 10582–10596, https://doi.org/10.1021/nn403743b.
[40] H.J. Kwon, M.-Y. Cha, D. Kim, D.K. Kim, M. Soh, K. Shin, T. Hyeon, I. Mook-Jung, Mitochondria-targeting ceria nanoparticles as antioxidants for Alzheimer's disease, ACS Nano 10 (2) (2016) 2860–2870, https://doi.org/10.1021/acsnano.5b08045.
[41] W. DeCoteau, K.L. Heckman, A.Y. Estevez, K.J. Reed, W. Costanzo, D. Sandford, P. Studlack, J. Clauss, E. Nichols, J. Lipps, M. Parker, B. Hays-Erlichman, J.C. Leiter, J.S. Erlichman, Cerium oxide nanoparticles with antioxidant properties ameliorate strength and prolong life in mouse model of amyotrophic lateral sclerosis, Nanomedicine 12 (8) (2016) 2311–2320, https://doi.org/10.1016/j.nano.2016.06.009.
[42] R. Najafi, A. Hosseini, H. Ghaznavi, S. Mehrzadi, A.M. Sharifi, Neuroprotective effect of cerium oxide nanoparticles in a rat model of experimental diabetic neuropathy, Brain Res. Bull. 131 (2017) 117–122, https://doi.org/10.1016/j.brainresbull.2017.03.013.
[43] Z.S. Bailey, A. Oyalowo, V.S.S.S. Sajja, B. Dunn, A. Hermundstad, P.J. VandeVord, E. Nilson, J.A. Bates, K.S. Hockey, C. Thorpe, H. Rogers, A.S. Frey, M.J. Billings, C.A. Sholar, B.A. Rzigalinski, C. Kumar, Cerium oxide nanoparticles improve outcome after *in vitro* and *in vivo* mild traumatic brain injury, J. Neurotrauma 33 (2016), https://doi.org/10.1089/neu.2016.4644.
[44] M.A. Hegazy, H.M. Maklad, D.M. Samy, D.A. Abdelmonsif, B.M. El Sabaa, F.Y. Elnozahy, Cerium oxide nanoparticles could ameliorate behavioral and neurochemical impairments in 6-hydroxydopamine induced Parkinson's disease in rats, Neurochem. Int. 108 (2017) 361–371, https://doi.org/10.1016/j.neuint.2017.05.011.
[45] H.J. Kwon, D. Kim, K. Seo, Y.G. Kim, S.I. Han, T. Kang, M. Soh, T. Hyeon, Ceria nanoparticle systems for selective scavenging of mitochondrial, intracellular, and extracellular reactive oxygen species in Parkinson's disease, Angew. Chem. Int. Ed. 57 (30) (2018) 9408–9412, https://doi.org/10.1002/anie.201805052.
[46] D.-W. Kang, C.K. Kim, H.-G. Jeong, M. Soh, T. Kim, I.-Y. Choi, S.-K. Ki, D.Y. Kim, W. Yang, T. Hyeon, S.-H. Lee, Biocompatible custom ceria nanoparticles against reactive oxygen species resolve acute inflammatory reaction after intracerebral hemorrhage, Nano Res. 10 (8) (2017) 2743–2760, https://doi.org/10.1007/s12274-017-1478-6.
[47] S. Lung, F.R. Cassee, I. Gosens, A. Campbell, Brain suppression of AP-1 by inhaled diesel exhaust and reversal by cerium oxide nanoparticles, Inhal. Toxicol. 26 (10) (2014) 636–641, https://doi.org/10.3109/08958378.2014.948651.
[48] R.G.S.V. Prasad, R. Davan, S. Jothi, A.R. Phani, D.B. Raju, Cerium oxide nanoparticles protects gastrointestinal mucosa from ethanol induced gastric ulcers in *in-vivo* animal model, Nano Biomed. Eng. 5 (2013) 46–49, https://doi.org/10.5101/nbe.v5i1.p46-49.
[49] D. Golyshkin, N. Kobyliak, O. Virchenko, T. Falalyeyeva, T. Beregova, L. Ostapchenko, M. Caprnda, L. Skladany, R. Opatrilova, L. Rodrigo, P. Kruzliak, A. Shcherbokov, M. Spivak, Nanocrystalline cerium dioxide efficacy for prophylaxis of erosive and ulcerative lesions in the gastric mucosa of rats induced by stress, Biomed. Pharmacother. 84 (2016) 1383–1392, https://doi.org/10.1016/j.biopha.2016.10.060.
[50] D. Oró, T. Yudina, G. Fernández-Varo, E. Casals, V. Reichenbach, G. Casals, B. González de la Presa, S. Sandalinas, S. Carvajal, V. Puntes, W. Jiménez, Cerium oxide nanoparticles reduce steatosis, portal hypertension and display anti-inflammatory properties in rats with liver fibrosis, J. Hepatol. 64 (3) (2016) 691–698, https://doi.org/10.1016/j.jhep.2015.10.020.
[51] M.R. Khaksar, M. Rahimifard, M. Baeeri, S. Hassani, S. Moeini-Nodeh, A. Kebriaeezadeh, F. Maqbool, M. Navaei-Nigjeh, M. Abdollahi, Protective effects of cerium oxide and yttrium oxide nanoparticles on reduction of oxidative stress induced by sub-acute exposure to diazinon in the rat pancreas, J. Trace Elem. Med. Biol. 41 (2017) 79–90, https://doi.org/10.1016/j.jtemb.2017.02.013.
[52] N.D.P.K. Manne, R. Arvapalli, V.A. Graffeo, V.V.K. Bandarupalli, T. Shokuhfar, S. Patel, K.M. Rice, G.K. Ginjupalli, E.R. Blough, Prophylactic treatment with cerium oxide nanoparticles attenuate hepatic ischemia reperfusion injury in Sprague Dawley rats, Cell. Physiol. Biochem. 42 (5) (2017) 1837–1846, https://doi.org/10.1159/000479540.
[53] A. Rocca, S. Moscato, F. Ronca, S. Nitti, V. Mattoli, M. Giorgi, G. Ciofani, Pilot *in vivo* investigation of cerium oxide nanoparticles as a novel anti-obesity pharmaceutical formulation, Nanomedicine 11 (7) (2015) 1725–1734, https://doi.org/10.1016/j.nano.2015.05.001.
[54] N. Kobyliak, O. Virchenko, T. Falalyeyeva, M. Kondro, T. Beregova, P. Bodnar, O. Shcherbakov, R. Bubnov, M. Caprnda, D. Delev, J. Sabo, P. Kruzliak, L. Rodrigo, R. Opatrilova, M. Spivak, Cerium dioxide nanoparticles possess anti-inflammatory properties in the conditions of the obesity-associated NAFLD in rats, Biomed. Pharmacother. 90 (2017) 608–614, https://doi.org/10.1016/j.biopha.2017.03.099.
[55] Z.-H. Zhang, R. Balasubramanian, Effects of cerium oxide and ferrocene nanoparticles addition as fuel-borne catalysts on diesel engine particulate emissions: Environmental and health implications, Environ. Sci. Technol. 51 (8) (2017) 4248–4258, https://doi.org/10.1021/acs.est.7b00920.
[56] D.O. Raemy, L.K. Limbach, B. Rothen-Rutishauser, R.N. Grass, P. Gehr, K. Birbaum, C. Brandenberger, D. Günther, W.J. Stark, Cerium oxide nanoparticle uptake kinetics from the gas-phase into lung cells *in vitro* is transport limited, Eur. J. Pharm. Biopharm. 77 (3) (2011) 368–375, https://doi.org/10.1016/j.ejpb.2010.11.017.
[57] J.Y. Ma, R.R. Mercer, M. Barger, D. Schwegler-Berry, J. Scabilloni, J.K. Ma, V. Castranova, Induction of pulmonary fibrosis by cerium oxide nanoparticles, Toxicol. Appl. Pharmacol. 262 (3) (2012) 255–264, https://doi.org/10.1016/j.taap.2012.05.005.
[58] S. Aalapati, S. Ganapathy, S. Manapuram, G. Anumolu, B.M. Prakya, Toxicity and bio-accumulation of inhaled cerium oxide nanoparticles in CD1 mice, Nanotoxicology 8 (7) (2013) 786–798, https://doi.org/10.3109/17435390.2013.829877.
[59] D. Schwotzer, H. Ernst, D. Schaudien, H. Kock, G. Pohlmann, C. Dasenbrock, O. Creutzenberg, Effects from a 90-day inhalation toxicity study with cerium oxide and barium sulfate nanoparticles in rats, Part. Fibre Toxicol. 14 (1) (2017) 23, https://doi.org/10.1186/s12989-017-0204-6.
[60] Y. Morimoto, H. Izumi, Y. Yoshiura, T. Tomonaga, T. Oyabu, T. Myojo, K. Kawai, K. Yatera, M. Shimada, M. Kubo, K. Yamamoto, S. Kitajima, E. Kuroda, K. Kawaguchi, T. Sasaki, Pulmonary toxicity of well-dispersed cerium oxide

nanoparticles following intratracheal instillation and inhalation, J. Nanopart. Res. 17 (11) (2015) 1–16, https://doi.org/10.1007/s11051-015-3249-1.
[61] C. Guo, S. Robertson, R.J.M. Webber, A. Buckley, J. Warren, A. Hodgson, J.Z. Rappoport, K. Ignatyev, K. Meldrum, I. Römer, S. Macchiarulo, J.K. Chipman, T. Marczylo, M.O. Leonard, T.W. Gant, M.R. Viant, R. Smith, Pulmonary toxicity of inhaled nano-sized cerium oxide aerosols in Sprague-Dawley rats, Nanotoxicology 13 (6) (2019) 733–750, https://doi.org/10.1080/17435390.2018.1554751.
[62] T. Masui, H. Hirai, N. Imanaka, G. Adachi, T. Sakata, H. Mori, Synthesis of cerium oxide nanoparticles by hydrothermal crystallization with citric acid, J. Mater. Sci. Lett. 21 (6) (2002) 489–491, https://doi.org/10.1023/A:1015342925372.
[63] Y. Zhang, Y. Lin, C. Jing, Y. Qin, Formation and thermal decomposition of cerium-organic precursor for nanocrystalline cerium oxide powder synthesis, J. Dispersion Sci. Technol. 28 (7) (2007) 1053–1058, https://doi.org/10.1080/01932690701524091.
[64] M. Horie, K. Fujita, H. Kato, S. Endoh, K. Nishio, L.K. Komaba, A. Nakamura, A. Miyauchi, S. Kinugasa, Y. Hagihara, E. Niki, Y. Yoshida, H. Iwahashi, Association of the physical and chemical properties and the cytotoxicity of metal oxide nanoparticles: metal ion release, adsorption ability and specific surface area, Metallomics 4 (4) (2012) 350–360, https://doi.org/10.1039/c2mt20016c.
[65] P. Canoa, R. Simón-Vázquez, J. Popplewell, Á. González-Fernández, A quantitative binding study of fibrinogen and human serum albumin to metal oxide nanoparticles by surface plasmon resonance, Biosens. Bioelectron. 74 (2015) 376–383, https://doi.org/10.1016/j.bios.2015.05.070.
[66] J. Gagnon, K.M. Fromm, Toxicity and protective effects of cerium oxide nanoparticles (nanoceria) depending on their preparation method, particle size, cell type, and exposure route, Eur. J. Inorg. Chem. 2015 (27) (2015) 4510–4517, https://doi.org/10.1002/ejic.201500643.
[67] H.-X. Mai, L.-D. Sun, Y.-W. Zhang, R. Si, W. Feng, H.-P. Zhang, H.-C. Liu, C.-H. Yan, Shape-selective synthesis and oxygen storage behavior of ceria nanopolyhedra, nanorods, and nanocubes, J. Phys. Chem. B 109 (51) (2005) 24380–24385, https://doi.org/10.1021/jp055584b.
[68] C. Veranitisagul, A. Kaewvilai, S. Sangngern, W. Wattanathana, S. Suramitr, N. Koonsaeng, A. Laobuthee, Novel recovery of nano-structured ceria (CeO_2) from Ce(III)-benzoxazine dimer complexes via thermal decomposition, Int. J. Mol. Sci. 12 (2011) 4365–4377, https://doi.org/10.3390/ijms12074365.
[69] M.R.C. Marques, R. Loebenberg, M. Almukainzi, Simulated biological fluids with possible application in dissolution testing, Dissolution Technol. 18 (3) (2011) 15–28, https://doi.org/10.14227/DT180311P15.
[70] H. Jogia, S.P. Sola, L.K. Garg, S. Arutla, A.M. Reddy, V. Venkateswarlu, A simple, safe, and environmentally friendly method of FaSSIF and FeSSIF preparation without methylene chloride, Dissolution Technol. 21 (1) (2014) 45–48, https://doi.org/10.14227/DT210114P45.
[71] E. Jantratid, N. Janssen, C. Reppas, J.B. Dressman, Dissolution media simulating conditions in the proximal human gastrointestinal tract: An update, Pharm. Res. 25 (7) (2008) 1663–1676, https://doi.org/10.1007/s11095-008-9569-4.
[72] M. Horie, K. Nishio, K. Fujita, S. Endoh, A. Miyauchi, Y. Saito, H. Iwahashi, K. Yamamoto, H. Murayama, H. Nakano, N. Nanashima, E. Niki, Y. Yoshida, Protein adsorption of ultrafine metal oxide and its influence on cytotoxicity toward cultured cells, Chem. Res. Toxicol. 22 (2009) 543–553, https://doi.org/10.1021/tx800289z.
[73] V. Paromov, M. Qui, H. Yang, M. Smith, W.L. Stone, The influence of N-acetyl-L-cysteine on oxidative stress and nitric oxide synthesis in stimulated macrophages treated with a mustard gas analogue, BMC Cell Biol. 9: No (2008) pp. given, https://doi.org/10.1186/1471-2121-9-33.
[74] B. Wang, P. Wu, R.A. Yokel, E.A. Grulke, Influence of surface charge on lysozyme adsorption to ceria nanoparticles, Appl. Surf. Sci. 258 (2012) 5332–5341, https://doi.org/10.1016/j.apsusc.2012.01.142.
[75] D.G. Dalgleish, Casein micelles as colloids: surface structures and stabilities, J. Dairy Sci. 81 (11) (1998) 3013–3018, https://doi.org/10.3168/jds.S0022-0302(98)75865-5.
[76] W.J. Donnelly, G.P. McNeill, W. Buchheim, T.C.A. McGann, A comprehensive study of the relationship between size and protein composition in natural bovine casein micelles, Biochim. Biophys. Acta, Protein Struct. Mol. Enzymol. 789 (2) (1984) 136–143, https://doi.org/10.1016/0167-4838(84)90197-3.
[77] E.K. Goharshadi, S. Samiee, P. Nancarrow, Fabrication of cerium oxide nanoparticles: Characterization and optical properties, J. Colloid Interface Sci. 356 (2) (2011) 473–480, https://doi.org/10.1016/j.jcis.2011.01.063.
[78] J.T. Dahle, K. Livi, Y. Arai, Effects of pH and phosphate on CeO_2 nanoparticle dissolution, Chemosphere 119 (2015) 1365–1371, https://doi.org/10.1016/j.chemosphere.2014.02.027.
[79] R.A. Yokel, M.L. Hancock, E.A. Grulke, J.M. Unrine, A.K. Dozier, U.M. Graham, Carboxylic acids accelerate acidic environment-mediated nanoceria dissolution, Nanotoxicology 13 (4) (2019) 466–475, https://doi.org/10.1080/17435390.2018.1553251.
[80] L. Otero-Gonzalez, I. Barbero, J.A. Field, F. Shadman, R. Sierra-Alvarez, Stability of alumina, ceria, and silica nanoparticles in municipal wastewater, Water Sci. Technol. 70 (9) (2014) 1533–1539, https://doi.org/10.2166/wst.2014.408.
[81] G. Chen, Z. Ni, Y. Bai, Q. Li, Y. Zhao, The role of interactions between abrasive particles and the substrate surface in chemical-mechanical planarization of Si-face 6H-SiC, RSC Adv. 7 (28) (2017) 16938–16952, https://doi.org/10.1039/C6RA27508G.
[82] K. Van Hoecke, J.T.K. Quik, J. Mankiewicz-Boczek, K.A.C. De Schamphelaere, A. Elsaesser, P. Van der Meeren, C. Barnes, G. McKerr, C. Vyvyan Howard, D. Van De Meent, K. Rydzynski, K.A. Dawson, A. Salvati, A. Lesniak, I. Lynch, G. Silversmit, B. De Samber, L. Vincze, C.R. Janssen, Fate and effects of CeO_2 nanoparticles in aquatic ecotoxicity tests, Environ. Sci. Technol. 43 (12) (2009) 4537–4546, https://doi.org/10.1021/es9002444.
[83] S.W. Mayer, S.D. Schwartz, The association of cerous ion with sulfite, phosphate, and pyrophosphate ions, J. Am. Chem. Soc. 72 (1950) 5106–5110, https://doi.org/10.1021/ja01167a080.
[84] I.A. Lebedev, Y.M. Kulyako, Study of the complexing of cerium(III) and cerium(IV) in concentrated phosphoric acid solutions, Zh. Neorg. Khim. 23 (12) (1978) 3215–3224.
[85] K. Li, S. Zhao, J. Ma, Study on solubility of cerium (IV) phosphate, J. Rare Earths 23 (1) (2005) 51–53.
[86] S. Lu, W. Zhang, R. Zhang, P. Liu, Q. Wang, Y. Shang, M. Wu, K. Donaldson, Q. Wang, Comparison of cellular toxicity caused by ambient ultrafine particles and engineered metal oxide nanoparticles, Part. Fibre Toxicol. 12 (2015) 1–24, https://doi.org/10.1186/s12989-015-0082-8.
[87] X. Zhou, B. Wang, Y. Chen, Z. Mao, C. Gao, Uptake of cerium oxide nanoparticles and their influences on functions of A549 cells, J. Nanosci. Nanotechnol. 13 (1) (2013) 204–215, https://doi.org/10.1166/jnn.2013.6788.
[88] S. Men, X. Cao, Z. Wang, Comparative study about cytotoxicity with CuO engineered nanoparticles, TiO_2 engineered nanoparticles, CeO_2 engineered nanoparticles, single-walled carbon nanotubes, Adv. Mater. Res. (Durnten-Zurich, Switz.) (2014) 881–883, https://doi.org/10.4028/www.scientific.net/AMR.881-883.956.
[89] L. De Marzi, A. Monaco, J. De Lapuente, D. Ramos, M. Borras, M. Di Gioacchino, S. Santucci, A. Poma, Cytotoxicity and genotoxicity of ceria nanoparticles on different cell lines *in vitro*, Int. J. Mol. Sci. 14 (2013) 3065–3077, https://doi.org/10.3390/ijms14023065.
[90] D. Speed, P. Westerhoff, R. Sierra-Alvarez, R. Draper, P. Pantano, S. Aravamudhan, K.L. Chen, K. Hristovski, P. Herckes, X. Bi, Y. Yang, C. Zeng, L. Otero-Gonzalez, C. Mikoryak, B.A. Wilson, K. Kosaraju, M. Tarannum, S. Crawford, P. Yi, X. Liu, S.V. Babu, M. Moinpour, J. Ranville, M. Montano, C. Corredor, J. Posner, F. Shadman, Physical, chemical, and *in vitro* toxicological characterization of nanoparticles in chemical mechanical planarization suspensions used in the semiconductor industry: towards environmental health and safety assessments, Environ. Sci.: Nano 2 (3) (2015) 227–244, https://doi.org/10.1039/C5EN00046G.
[91] W. Lin, Y.W. Huang, X.D. Zhou, Y. Ma, Toxicity of cerium oxide nanoparticles in human lung cancer cells, Int. J. Toxicol. 25 (6) (2006) 451–457, https://doi.org/10.1080/10915810600959543.
[92] S. Lanone, F. Rogerieux, J. Geys, A. Dupont, E. Maillot-Marechal, J. Boczkowski, G. Lacroix, P. Hoet, Comparative toxicity of 24 manufactured nanoparticles in human alveolar epithelial and macrophage cell lines, Part. Fibre Toxicol. 6 (2009), https://doi.org/10.1186/1743-8977-6-14.
[93] M. Horie, K. Nishio, H. Kato, K. Fujita, S. Endoh, A. Nakamura, A. Miyauchi, S. Kinugasa, K. Yamamoto, E. Niki, Y. Yoshida, Y. Hagihara, H. Iwahashi, Cellular responses induced by cerium oxide nanoparticles: induction of intracellular calcium level and oxidative stress on culture cells, J. Biochem. 150 (2011) 461–471, https://doi.org/10.1093/jb/mvr081.
[94] Y. Ma, S. Elankumaran, L.C. Marr, E.P. Vejerano, A. Pruden, Toxicity of engineered nanomaterials and their transformation products following wastewater treatment on A549 human lung epithelial cells, Toxicol. Rep. 1 (2014) 871–876, https://doi.org/10.1016/j.toxrep.2014.08.017.
[95] S.-G. Shen, H.-L. Liu, W.-Y. Wang, G.-Q. Gu, G.-Q. Zhou, [Protection effects of CeO_2 nanoparticles on A549 cells], Hebei Daxue Xuebao Ziran Kexueban 31 (2) (2011) 160–166.
[96] L. Vila, A. Garcia-Rodriguez, C. Cortes, A. Velazquez, N. Xamena, A. Sampayo-Reyes, R. Marcos, A. Hernandez, Effects of cerium oxide nanoparticles on differentiated/undifferentiated human intestinal Caco-2 cells, Chem. Biol. Interact. 283 (2018) 38–46, https://doi.org/10.1016/j.cbi.2018.01.018.
[97] A.K. Hauser, E.F. Daley, K.W. Anderson, M.I. Mitov, R.C. McGarry, J.Z. Hilt, Targeted iron oxide nanoparticles for the enhancement of radiation therapy, Biomaterials 105 (2016) 127–135, https://doi.org/10.1016/j.biomaterials.2016.07.032.
[98] M. Decleer, J. Jovanovic, A. Vakula, B. Udovicki, R.-S.E.K. Agoua, A. Madder, S. De Saeger, A. Rajkovic, Oxygen consumption rate analysis of mitochondrial dysfunction caused by *Bacillus cereus* cereulide in Caco-2 and HepG2 Cells, Toxins (Basel) 10 (7) (2018), https://doi.org/10.3390/toxins10070266 266/1-266/15.
[99] B.K. Gaiser, T.F. Fernandes, M.A. Jepson, J.R. Lead, C.R. Tyler, M. Baalousha, A. Biswas, G.J. Britton, P.A. Cole, B.D. Johnston, Y. Ju-Nam, P. Rosenkranz, T.M. Scown, V. Stone, Interspecies comparisons on the uptake and toxicity of silver and cerium dioxide nanoparticles, Environ. Toxicol. Chem. 31 (1) (2012) 144–154, https://doi.org/10.1002/etc.703.
[100] B. Park, K. Donaldson, R. Duffin, L. Tran, F. Kelly, I. Mudway, J.P. Morin, R. Guest, P. Jenkinson, Z. Samaras, M. Giannouli, H. Kouridis, P. Martin, Hazard and risk assessment of a nanoparticulate cerium oxide-based diesel fuel additive - a case study, Inhal. Toxicol. 20 (6) (2008) 547–566, https://doi.org/10.1080/08958370801915309.
[101] M.N. Shepard, S. Brenner, An occupational exposure assessment for engineered nanoparticles used in semiconductor fabrication, Ann. Occup. Hyg. 58 (2) (2014) 251–265, https://doi.org/10.1093/annhyg/met064.
[102] R. Landsiedel, L. Ma-Hock, K. Wiench, S. Gröters, B. van Ravenzwaay, H. Ernst, D. Schaudien, Long-term effects of inhaled nanoparticles in rats: Ceriumdioxide and bariumsulphate. The Toxicologist, Suppl. Toxicol. Sci. 168 (1) (2019) Abstract # 2217.
[103] K.P. Strohl, A.J. Thomas, J.P. St, E.H. Schlenker, R.J. Koletsky, N.J. Schork, Ventilation and metabolism among rat strains, J. Appl. Physiol. 82 (1) (1997) 317–323, https://doi.org/10.1152/jappl.1997.82.1.317.